

GEOLOGY FOR SOCIETY

SINCE 1858



**GEOLOGICAL
SURVEY OF
NORWAY**

· NGU ·

Report no.: 2019.026		ISSN: 0800-3416 (print) ISSN: 2387-3515 (online)		Grading: Open
Title: Magnetotelluric measurements in the Rondane region, southern Norway during two field campaigns (2017- 2018)				
Authors: Maxim Yu. Smirnov, Sofie Gradmann, Odleiv Olesen & Arne Bjørlykke			Client: Geological Survey of Norway and Luleå University of Technology	
County: Innlandet			Municipality: Stor-Elvdal, Folldal, Dovre, Sel, Nord-Fron, Sør-Fron, Ringebu	
Map-sheet name (M=1:250.000) Lillehammer, Røros, Ålesund, Årdal			Map-sheet no. and -name (M=1:50.000)	
Deposit name and grid-reference:			No. pages: 36 Price (NOK): Map enclosures:	
Fieldwork carried out: 2017-2018		Date of report: 19.12.2019		Project no.: 3622.00
Person responsible: 				
<p>New magnetotelluric (MT) data were acquired in the southern Scandinavian mountains to study the crustal structure of the Late Caledonian Gudbrandsdalen Anticline including the Atnsjø tectonic window and the adjacent Middle and Upper Allochthon. The project focuses on investigating the structure of the upper Precambrian basement in the area related to the Western Gneiss Region (WGR), surrounded by the Caledonian nappes. One problem we are addressing is the depth extension of the Devonian detachments related to the late Caledonian gravity collapse and their influence on the old passive continental margin beneath the Caledonian Orogen.</p> <p>During the first field campaign (September 2017) a total of 33 broad-band magnetotelluric sites were acquired. The signal to noise ratio was relatively high due to significant geomagnetic activity at the time of the measurement. This resulted in a good quality of the measured time series, especially in the so-called dead-band between 0.1 and 10 s, where the geomagnetic activity is usually low except during geomagnetic sub-storms. Consequently, improvements in final estimates of magnetotelluric transfer functions are clearly noticeable. We estimated MT transfer functions in the period range from 0.003 to 1000 s. The principal direction of the impedance tensor can be identified for the periods longer 0.1 s; however, it varies with period. For the data inversion, we firstly chose to invert in 2D the determinant of the impedance tensor, which mitigates 3D effects under 2D model assumptions. Three crustal-scale 2D models were selected and analysed for the data from the first field campaign.</p> <p>In order to get a better understanding of the regional structures and to connect to the previously measured ToSca profile (2010), we conducted another field measurement in the summer of 2018. Additional 32 sites were added, totalling 65 sites acquired within the project. The data from 2018 have a somewhat lower quality compared to the data collected the previous year. There were more sites installed in populated areas with a lot of agricultural activity, including, for example, numerous electric fences for animals. Overall the data quality for the accepted sites from both field campaigns varies from good to excellent.</p> <p>Due to the fact that the data mostly exhibit a 3D behaviour (like in most real situations) we prefer to use full impedance tensor for 3D inversion. First of all, this allows us to use all the available data (all impedance components) and, secondly, it does not require to make assumptions about dimensionality. The 3D inversion resulted in a good data fit. Hence, we base our interpretation on the results of the 3D inversions primarily. Various sensitivity tests, involving 3D inversion runs with different parameters, support the main features of the resulting model.</p> <p>The final 3D electrical conductivity model reveals highly resistive crustal block, extending to the surface, imaging the parautochthonous Western Gneiss Region. In ToSca'10, the Caledonian nappes, the conducting Neo-Proterozoic Brøttum Formation and the Cambrian-Ordovician Alum Shale Formation and the deeper conductors are terminated in the west by the late Devonian detachments (Faltungsgaben shear complex and Agdenes detachment), which represent a crustal scale boundary between the Western Gneiss Region in the west and the Southwest Scandinavian Domain in the east. This behaviour is confirmed in the new model. However, its 3D behaviour and more complex structure are also more evident than it was inferred before. The Gudbrandsdalen Anticline within the Middle Allochthon is clearly identified as an E-W striking resistive feature through the entire model domain. Upper and lower allochthons are more conductive at nearly the entire crustal scale. The focus of our study, the Atnsjø tectonic window appears to be the part of resistive Middle Allochthon and the Gudbrandsdal Anticline and cannot be separated from it based on the conductivity model alone. We conclude that highly conductive black schists and alum shales are absent in the Atnsjø tectonic window.</p>				
Keywords: Geofysikk (Geophysics)		Magnetotellurikk (Magnetotellurics)		Tolkning (Interpretation)
Berggrunnsgeologi (Bedrock geology)		Prosessering (Processing)		Kaledonidene (Caledonides)
Flymåling (Fixed-wing measurements)				Fagrapport (Scientific report)



Contents

1. Introduction	3
2. Geology of the study area	3
3. Data acquisition	6
4. Data processing	8
5. Data Analysis	11
6. 2D inversion	13
7. Discussion and conclusions	19
8. References	21
9. Appendices	24
9.1. Appendix A	24
9.2. Appendix B	29

1. Introduction

Previous magnetotelluric array ToSca10 (Fig.1) covers the area from the Southwest Scandinavian Domain (SSD) in the east, across the Caledonides to the Western Gneiss Region (WGR) in western Norway. The study revealed the following features in the final 2D conductivity model (Cherevatova et al., 2014):

- the Precambrian basement (autochthonous SSD and parautochthonous WGR, with respect to the Caledonian orogen) is generally resistive;
- the western part of WGR is more conductive possibly due to a large-scale shearing during to the post-Caledonian extension;
- the SSD contains several sub-horizontal layers, the high conductivity of which implies an electronic conduction mechanism (graphite, sulphides);
- the mid-crustal conductors in the SSD represent the remnants of closed basins (e.g., peripheral foreland basins, retroarc basins, back-arc basins) formed during the accretions and collisions of various Sveconorwegian terranes;
- the shallower conductors represent highly conducting Late Precambrian to Early Palaeozoic shallow-sea sediments, the so-called Alum Shale Formation of Late Cambrian-Early Ordovician age and the black schists of Late Proterozoic age (Brøttum Formation), that mark the boundary between the Precambrian basement and the overlying Caledonian nappes and partly represent a decollement along which the Caledonian nappes were overthrust.

Based on these findings, we aim in the project to explore the deep structure of the Gudbrandsdalen Anticline and the deformed Atnsjø tectonic window using the magnetotelluric method. The magnetotelluric method is a passive geophysical electromagnetic method aiming to study the conductivity of the subsurface. Due to its nature, it allows obtaining depth information from the surface down to a few hundreds of km. Following the conductive structures at depth in the area, we anticipate getting a better picture of the deformed Atnsjø tectonic window. In the following sections, we have a short description of the geology, general methodology, data analysis and inversion technique.

2. Geology of the study area

The area of investigation in southern Norway is surrounded by, from the oldest to the youngest formations of the Southwest Scandinavian Domain (SSD), the Western Gneiss Region (WGR), the Caledonides, and the Oslo Graben (Fig. 1). The Scandinavian Caledonides (Fig. 1) were formed as the result of a closure of the Iapetus Ocean and a continental collision of Baltica and Laurentia in the Late Silurian (Gorbatshev & Bogdanova, 1993; Rykkelid & Andresen, 1994; Roberts, 2003; Gee et al., 2008; Ramberg et al., 2008). In the Caledonian orogeny (540-400 Ma), the Precambrian rocks in the western margin of Baltica were thrust beneath Laurentia to ultra-high-pressure depths. The underthrust rocks of the Baltica were heated, metamorphosed and deformed (Andersen, 1998) whereas the rocks of the Neoproterozoic to Early Palaeozoic accretionary wedge were transported to the east/northeast over Baltica as the Caledonian nappes. The Caledonian nappes are generally divided into lower, middle, upper and uppermost allochthons (nappe series) (Törnebohm, 1896; Gee & Sturt, 1985; Andersen,

1998; Roberts, 2003; Ramberg et al., 2008; Gee et al., 2008; Stratford & Thybo, 2011). The major nappe thrusting was completed between 400 and 405 million years ago. Today the remnants of the Caledonian orogen are preserved as a relatively thin cover above the Precambrian basement which stretches northeast from Ireland and Scotland in the south to Svalbard in the north (Ramberg et al., 2008). The Caledonian mountains have been deeply eroded since the Devonian. Late- to postorogenic extension in southern Norway resulted in penetrative reworking and decompression of the Caledonian high-pressure metamorphic rocks, the formation of large extensional detachments and the Devonian supra-detachment basins (Norton et al., 1987; Andersen, 1998). During these Devonian extensional tectonics, the Precambrian basement of the Sveconorwegian age was exhumed and drawn back towards the east now forming the parautochthonous WGR in western Norway.

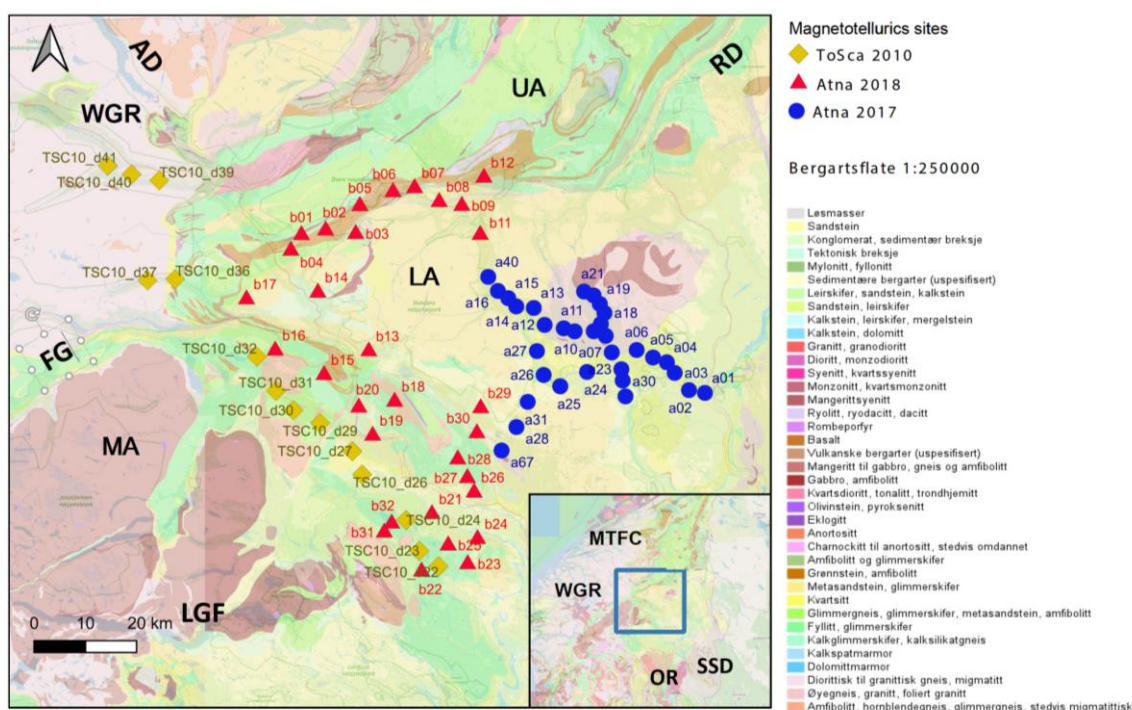


Figure 1: Main geological units of the Caledonian orogen and the Precambrian basement in south-western Fennoscandia, the location of the Rondane (ATNA) and ToSca 2010 magnetotelluric sites (2017 – blue circles; 2018 – red triangles; ToSca10 – olive green diamonds). Caledonian orogen: UA- Upper allochthon – greenstones, gabbros, mica schists from the lapetus Ocean (Neoproterozoic – Silurian); MA- Middle allochthon – basement nappes of Baltica origin (Mesoproterozoic – Cambrian); LA - Lower allochthon – sandstones, phyllites, mica schists, shales from the periphery of the Baltica basement (Mesoproterozoic – Palaeozoic); Parautochthon – shales, alum shales, sandstones and carbonate rocks, transformed during thrusting (Cambrian – Silurian); Parautochthonous basement (WGR) – Precambrian basement variably affected by the Caledonian orogeny; Autochthon – basement unaffected by the Caledonian extension (Neoproterozoic – Cambrian), SSD - Southwest Scandinavian Domain. Post-Caledonian extension: LGF – Lærdal-Gjende Fault, AD – Agdenes Detachment, RD – Røragen Detachment, FG – Faltungsgraben shear complex, MTFC – Møre-Trøndelag Fault Complex (Devonian-Jurassic), OR – Oslo Rift (mainly Permian). The map is compiled and simplified after Ramberg et al. (2008). Remote reference sites b03 and a29 are marked.

The rocks of WGR subducted to ultra-high pressure conditions and subsequently exposed to the surface represent a particular interest and are a target of the study within the current project. The present structure of the Scandinavian Caledonides is strongly influenced by extensional shear zone complexes, e.g. Faltungsgraben (FG), the Lærdal-

Gjende Fault in the SW, the Agdenes Detachment in the north and the Røragen Detachment in the NE, Møre-Trøndelag Fault Complex (MTFC) in the far NW and black schists having a carbon content up to 10% (Norton et al., 1987; Andersen, 1998; Ramberg et al., 2008; Robinson et al., 2014) . The latter, consisting partly of the c. 100 m thick Alum Shale, comprises one of the most widespread lithostratigraphic units in Scandinavia (Andersson et al., 1985; Bergström and Gee, 1985; Gee, 2005). The organic-rich alum shale beds provided a well-lubricated surface acting as a detachment plane for the nappes in the Caledonian orogeny along the length of the entire mountain belt (Gee, 1980, 2005). Black shales thus formed a parautochthon in the Caledonian orogeny above the basement rocks of the SSD that remained largely unaffected during the Caledonian orogeny, i.e. formed an indicating W- to NW- directed movement (Gee et al., 2008). The 4-5 km thick Neo-Proterozoic Brøttum Formation (Ramberg et al., 2008) consists to a large degree of black schists and was formed as turbidites in the Hedmark Basin in the southern part of the study area. The last phase of the Late Devonian to Middle Carboniferous Variscan orogeny to the south of Fennoscandia caused extensional rifting inside the orogeny and in the foreland to the north in the southern parts of Baltica (Norton et al., 1987; Andersen, 1998). The largest of these rifts was the 500 km long, NNE-SSW trending Oslo Rift (Graben) that is terminated in the south by the Sorgenfrei-Tornquist zone (Ramberg et al., 2008).

Fig. 2c shows the depth to the Precambrian basement in southeastern Norway (Bjørlykke & Olesen, 2018) based on interpretation of aeromagnetic and gravity data (Figs. 2a & b) as well as existing bedrock maps (Fig. 2d). The basement depression extending from Lillehammer to the north–northwest represents the southern extremity of a basement structure that hosted the Hedmark Basin. Within the zone of deformed basement there are three 3-4 km-deep basins/depressions named the Atna, Fåvang and Åsta basins (Fig. 2). The depressions are probably produced by Caledonian thrusting of the basement and are related to the transport of the Atnsjø window and the Osen–Røa Nappe Complex (Bjørlykke & Olesen, 2018).

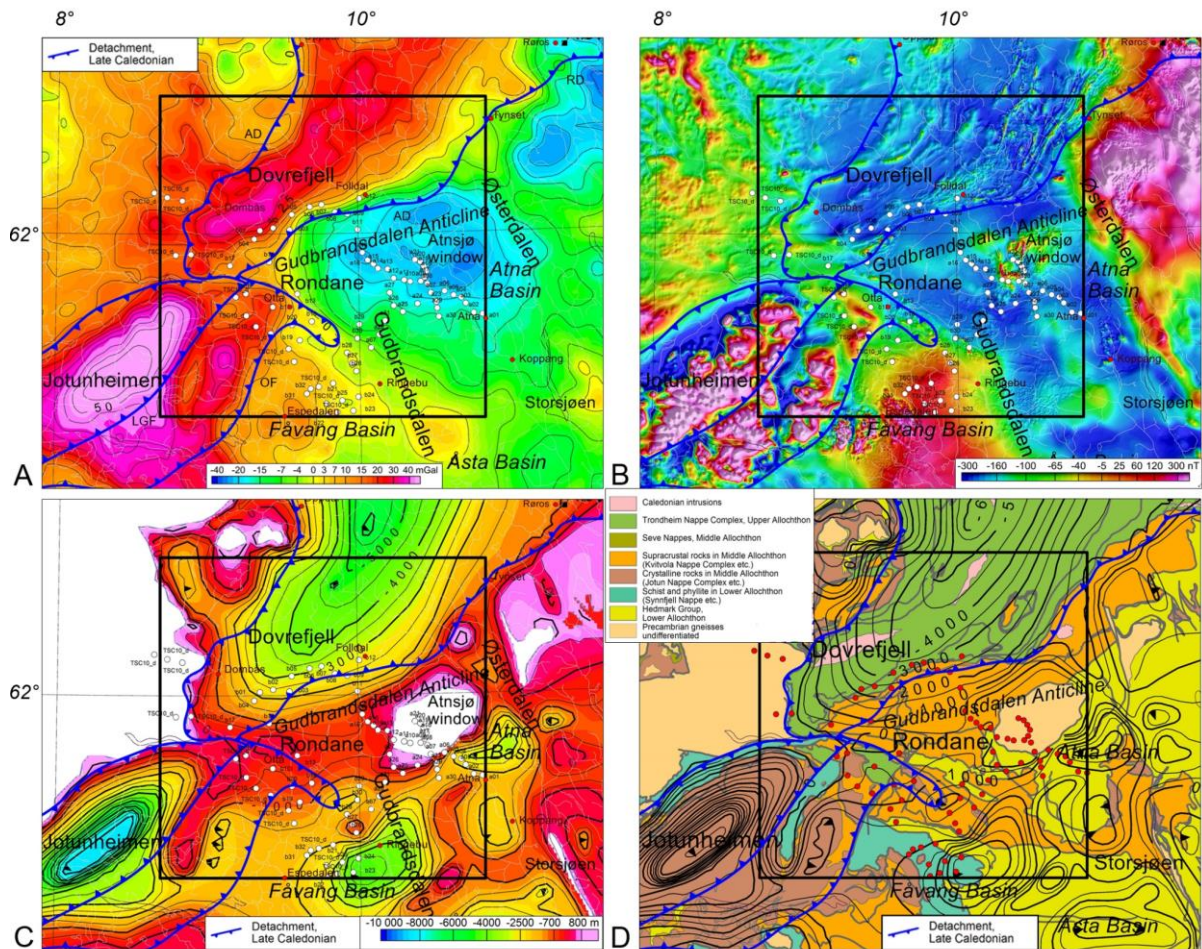


Figure 2: Gravity and aeromagnetic data and interpretations from the study area (modified from Bjørlykke and Olesen, 2018). The black frames show the location of Fig. 10. The MT stations are shown as white circles in Figs. A, B and C and as red circles in Fig. D. Late-Caledonian detachments (modified from Norton et al., 1987; Robinson et al., 2014; Pérez, 2015) are shown as blue lines with the barbs towards the downthrown side: AD-Agdenes Detachment; RD-Røragen Detachment; LGF-Lærdal-Gjende Fault; OF-Olestøl Fault. A) Gravimetric isostatic residual map of central Norway and adjacent areas (Olesen et al., 2010). B) Aeromagnetic compilation (modified from Olesen et al., 2010). C) Depth to Precambrian basement in central and southeastern Norway based primarily on magnetic depth estimates by Knut Åm (in Nystuen, 1981) and gravity models in Jotunheimen and Trøndelag (Skilbrei et al., 2002; Mekonnen, 2004, respectively). D) Simplified tectonic map of central and eastern Norway based on Koistinen et al. (2001). The estimated depth to Precambrian basement is shown with black contours.

3. Data acquisition

The entire Rondane array covers approximately an area of 100x100 km (Fig. 1). The measurements commenced in September 2017 and were continued in the summer of 2018 resulting in 65 broad-band magnetotelluric (BMT) sites including two permanent reference stations (b03, a29), running the whole duration of the field work (for more than two weeks each). The average separation between BMT sites is about 3 km along accessible roads in the area (Table 1). We also used previously acquired data from the ToSca10 profile, which comprised a total of 78 sites available for 3D inversion. Broad-band MT data were collected in the frequency range from 0.003 to 1000 Hz with the MTU2000 MT system developed at Uppsala University, Sweden (Smirnov et al., 2008) and later using a new Metronix ADU08 system. The duration of recordings was usually

Site Name	Latitude	Longitude
TSC10_d22	61.442020	9.845800
TSC10_d23	61.468700	9.776570
TSC10_d24	61.521750	9.727560
TSC10_d26	61.600640	9.568080
TSC10_d27	61.640830	9.532480
TSC10_d29	61.689280	9.415700
TSC10_d30	61.711020	9.319160
TSC10_d31	61.744830	9.255490
TSC10_d32	61.803290	9.186450
TSC10_d36	61.936090	8.890150
TSC10_d37	61.933650	8.789780
TSC10_d39	62.103850	8.832210
TSC10_d40	62.114090	8.731550
TSC10_d41	62.128810	8.645060
a01	61.741090	10.812420
a02	61.745930	10.754430
a03	61.775380	10.702500
a04	61.793730	10.674170
a05	61.801790	10.624140
a06	61.814670	10.564540
a07	61.810500	10.474350
a08	61.839020	10.452260
a09	61.846760	10.408730
a10	61.846580	10.339530
a11	61.851820	10.299920
a12	61.857720	10.230520
a13	61.886730	10.191270
a14	61.889320	10.127690
a15	61.903430	10.098610
a16	61.915740	10.061000
a17	61.859320	10.434730
a18	61.878050	10.447600
a19	61.893590	10.430740
a20	61.908050	10.408280
a21	61.914720	10.373710
a23	61.781710	10.509060
a24	61.777110	10.384470
a25	61.752510	10.287310
a26	61.771930	10.227080
a27	61.812750	10.202700

Site Name	Latitude	Longitude
a27	61.812750	10.202700
a28	61.682430	10.128160
a29	61.762400	10.513810
a30	61.735240	10.523960
a31	61.725750	10.169210
a40	61.939690	10.026020
a67	61.642030	10.074420
a75	61.752510	10.287290
b01	62.011000	9.348180
b02	62.018860	9.435960
b03	62.012860	9.545050
b04	61.98428	9.30993
b05	62.060520	9.560050
b06	62.084163	9.680345
b07	62.090870	9.758780
b08	62.067315	9.84805
b09	62.060600	9.930300
b11	62.01152	9.9968167
b12	62.108520	10.010260
b13	61.81235	9.5926783
b14	61.912780	9.407820
b15	61.771870	9.430150
b16	61.813717	9.2529533
b17	61.901360	9.148840
b18	61.726	9.6863483
b19	61.667510	9.606530
b20	61.716020	9.556130
b21	61.532090	9.821770
b22	61.432765	9.78406
b23	61.445630	9.951460
b24	61.489050	9.987190
b25	61.478095	9.8807467
b26	61.569460	9.974770
b27	61.594610	9.950350
b28	61.626783	9.91553
b29	61.714870	9.998720
b30	61.671702	9.9848533
b31	61.500368	9.6487867
b32	61.515870	9.675500

Table 1. Coordinates of all measured sites during field campaigns 2017 (a-sites), 2018 (b-sites) and previously available sites in the area from 2010 (TSC10-sites)

one day (i.e., around 20 hours). Broad-band MT data were continuously sampled at 20 Hz and simultaneous burst recordings with 1000 Hz sampling were recorded for 2 hrs starting at midnight. A few sites located close to infrastructure were contaminated by cultural EM noise, that we successfully dealt with using robust remote reference processing, except one site. An example of time series sampled at 20Hz is shown in Fig. 3.

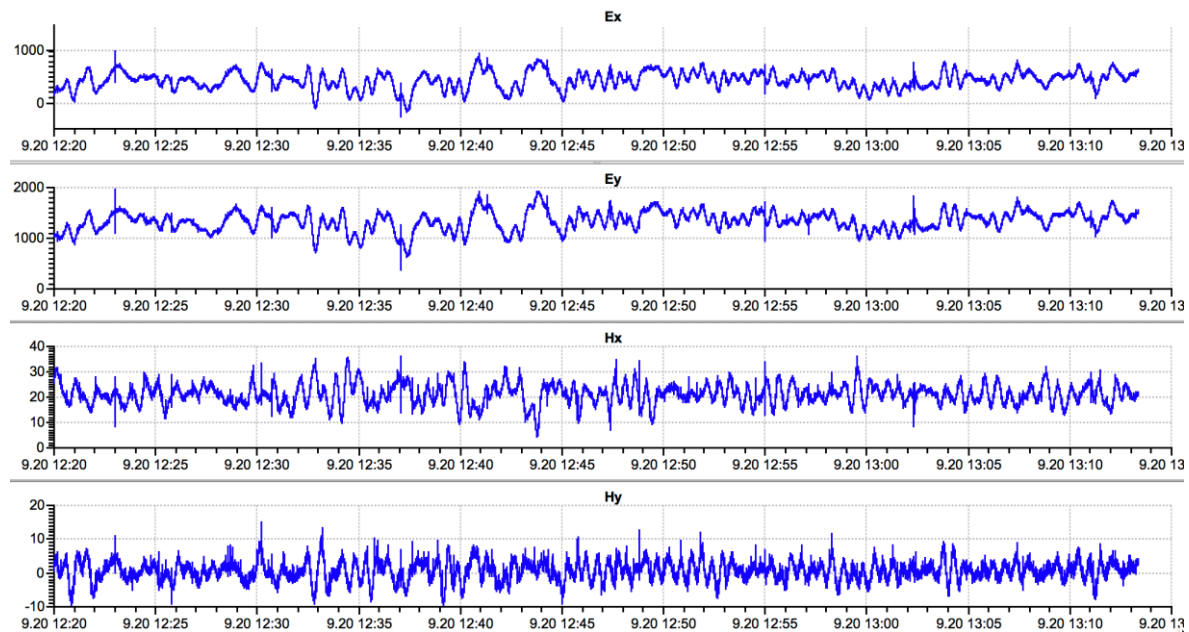


Figure 3: Time series of horizontal electromagnetic field components \mathbf{E} and \mathbf{H} sampled at 20 Hz. The site was located in the area with relatively low cultural noise. Geomagnetic Pc3 and Pc4 pulsations are clearly visible on the time series. The vertical scale is given in mV as recorded by the data logger (no deconvolution was applied before plotting the time series to remove system response).

4. Data processing

In magnetotellurics, it is assumed that the source field can be regarded as a homogeneous plane wave. This is an acceptable assumption as long as the penetration depth into the earth (penetration depth (skin depth) increases roughly as the square root of the period of oscillation) is smaller than the distance to the dominating current systems in the ionosphere, starting at the height of approximately 110 km. Under these assumptions, the following plane wave transfer functions can be defined in the frequency domain (Berdichevskiy & Dmitriev, 1976):

$$\mathbf{E}_h = \begin{Bmatrix} E_x \\ E_y \end{Bmatrix} = \begin{Bmatrix} Z_{xx} & Z_{xy} \\ Z_{yx} & Z_{yy} \end{Bmatrix} \begin{Bmatrix} H_x \\ H_y \end{Bmatrix} = \mathbf{Z}_h \mathbf{H}_h$$

where the horizontal magnetic field acts as input channels to the Earth's linear system described by the impedance tensor \mathbf{Z} , which is completely independent of the source structure and solely depends on underlying conductivity structure of the Earth's interior.

It is customary to represent the impedance elements in terms of apparent resistivity and phase defined as

$$\rho_{xy}^a = \frac{T}{2\pi\mu_0} |Z_{xy}|^2, \quad \rho_{yx}^a = \frac{T}{2\pi\mu_0} |Z_{yx}|^2 \quad \text{and} \quad \rho_{Det}^a = \frac{T}{2\pi\mu_0} |Z_{xx}Z_{yy} - Z_{xy}Z_{yx}| = \frac{T}{2\pi\mu_0} |Det|$$

and

$$\phi_{xy}^a = \tan^{-1} \left[\frac{\text{Im}(Z_{xy})}{\text{Re}(Z_{xy})} \right], \quad \phi_{yx}^a = -\tan^{-1} \left[\frac{\text{Im}(Z_{yx})}{\text{Re}(Z_{yx})} \right] \quad \text{and} \quad \phi_{Det}^a = \frac{1}{2} \tan^{-1} \left[\frac{\text{Im}(Det)}{\text{Re}(Det)} \right]$$

where T is the period in s, Det is the determinant (effective impedance) of the impedance tensor (Berdichevsky & Dmitriev, 1976). Apparent resistivities are often used to present the data, as well as to examine data fit from predicted transfer functions. It should be noted that a 2D model assumption relies on the existence of only two main off-diagonal components of the impedance tensor, while the diagonal components are zero. In realistic 3D situations, diagonal elements will never vanish and therefore have to be considered. Therefore, in 3D inversion, we usually try to fit the full impedance tensor, which also provides additional resolution power due to the increased amount of information in the data.

All the transfer functions were estimated using robust multi-remote reference technique (Smirnov, 2003) as well as novel multivariate analysis technique (Smirnov & Egbert, 2012), thus providing stable transfer function in the period range from 0.003-1000 s at all sites.

During data processing, the time series of horizontal components of electromagnetic field (e_x, e_y, h_x, h_y) recorded at the Earth's surface are being transformed into the impedance tensor (transfer function). We have also additionally estimated horizontal magnetic transfer function (perturbation tensor), relating horizontal magnetic components at local sites to the reference sites:

$$\begin{pmatrix} H_x^l \\ H_y^l \end{pmatrix} = \begin{bmatrix} M_{xx} & M_{xy} \\ M_{yx} & M_{yy} \end{bmatrix} \begin{pmatrix} H_x^r \\ H_y^r \end{pmatrix},$$

where index l stands for the local site and index r for the reference site. During the whole field campaign, we had one site recording at the same location permanently; therefore, we could employ it as a reference site to estimate the perturbation tensor. It should be noted that we did not use perturbation tensor for data inversions and therefore, do not describe it in more details. Further development of 3D inversion code is required in order to fully exploit all the available data.

The array is located at relatively high geomagnetic latitudes, where the plane wave assumptions might be violated by the close proximity of sources. Therefore, we have used the multivariate analysis to check for the presence of source field distortions in MT transfer functions. Data examples are shown in Figs. 4 and 5 for several sites. Multivariate estimates did not reveal any additional features in the data, which might be attributed to the source field effects. It was previously noted (Cherevatova et al., 2015) that those effects are usually not significant, if even noticeable. In general, apparent resistivities

show consistent behaviour among different sites, indicating similarities in the observed structure. While there are no significant anomalies observed in the data, static shift and near-surface distortions are noticeable in the data. We have used the following criteria to evaluate data quality and perform data selection. First, we discarded highly scattered impedance estimates having large error bars. We also checked that impedance tensor parameter, like skew values, phase tensor and strike are stable, varying smoothly with period. Secondly, apparent resistivity and phase should be consistent in order to satisfy dispersion relations which are proven to be valid for 1D and 2D TM-mode models (Berdichevsky & Pokhotelov, 1997). We used this relation as the last criterion for data selection. As it was mentioned above, the data quality is relatively high, and all the sites except one passed the quality check for 2D inversions (at few sites we have limited used period range). Larger error bars are often observed at longer periods due to the smaller size of the statistics available. Overall the data quality varies from good to excellent, providing a solid basis for the subsequent interpretation.

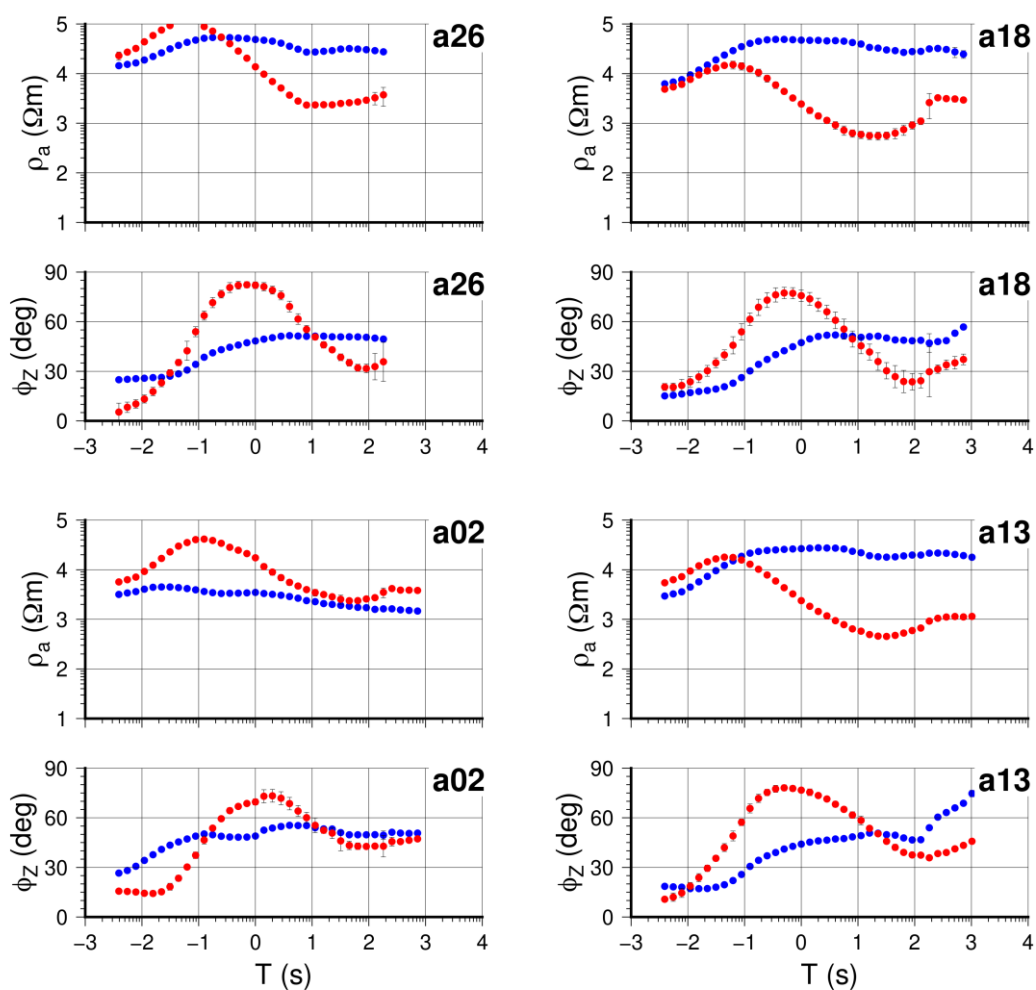


Figure 4: Example of data from 2017 field campaign. Estimated main components of the impedance tensor, shown as apparent resistivities and impedance phases. Apparent resistivities ρ_{xy} , ρ_{yx} are marked in red and blue circles, respectively, as well as the impedance phases ϕ_{xy} , ϕ_{yx} .

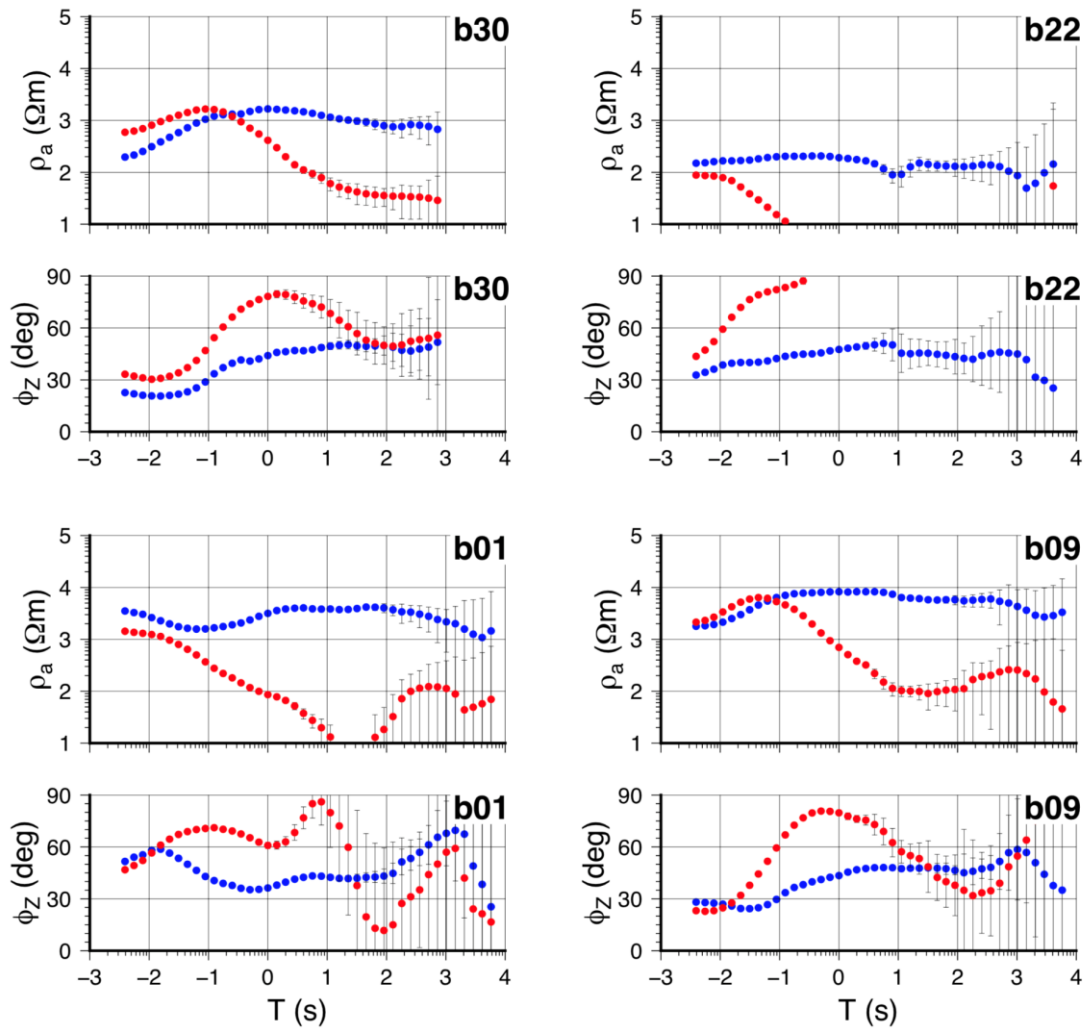


Figure 5: Example of data from 2018 field campaign. Estimated main components of the impedance tensor, shown as apparent resistivities and impedance phases. Apparent resistivities ρ_{xy} , ρ_{yx} are marked in red and blue circles, respectively, as well as the impedance phases ϕ_{xy} , ϕ_{yx} .

5. Data Analysis

The first step in the analysis of impedance tensors is to estimate the strike and dimensionality of the underlying structure. It is especially important when the 2D modelling assumption is used to interpret the data. However, it is not necessary to carry out the analysis if 3D inversion alone is considered. Nevertheless, the results of the analysis provide additional insight into the data quality and underlying structure and may assist in 3D inversion model grid construction (grid orientation). We have chosen to use phase tensor to evaluate strike and dimensionality. The phase tensor skew and rose histograms of principal directions of the impedance tensor are summarized for all sites as a function of period (Booker, 2014). Alternatively, other approaches could be used, like Q-analysis (Smirnov & Pedersen, 2009) or phase-sensitive parameters (Bahr, 1991). However, they provide similar information (but in various degree sensitive to noise and 3D effects).

The skew β of the phase tensor can be considered as a measure of 3D effects. When skew β is close to 0, the underlying structure can be described as 1D or 2D, perturbed by

small scale surface inhomogeneities effects which are frequency independent. In practice, a value of skew $\beta < 3^\circ$ (and this should be the case for a range of nearby frequencies and sites as well) has been used to justify 1D or 2D approaches (Booker, 2014). As can be seen from Fig. 5 our data set exhibits pronounced 3D effects. However, surprisingly all the sites have a rather consistent strike direction especially within this period band from 0.1 to 10 s, whilst at the same time skew values are even higher in this band. We could interpret this strong 3D effect as being caused by regional scale structures, therefore.

Despite the strong 3D imprints, the phase tensors show uniform orientations at longer periods in the N30E principle direction (Periods > 10 s). However, there are differences in strike direction for different period ranges, which is attributed to generally 3D data behaviour. The period range of $T < 10$ s is remarkable for having very stable, but a different strike of N60E deg compared to $T > 10$ s. It indicates that the direction towards the conductive anomaly is situated outside of the profile and is overall coincident with the direction of a central resistive region (RA). Due to the 90° ambiguity, it is not possible to detect (predict) the structure location, however taking into account ToSca10 results we could conclude that there are structures towards N120W, where major conductors were found.

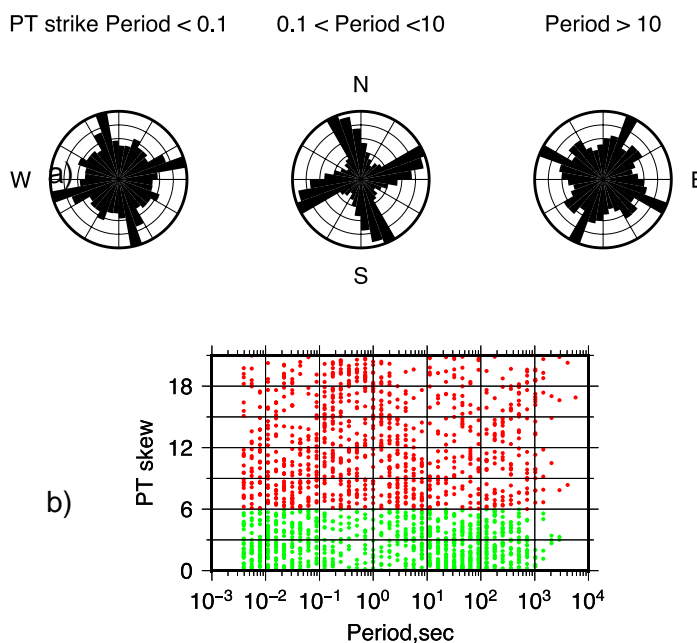


Figure 6: Results of strike and dimensionality analysis for all data from the Rondane 2017-2018 field survey as well as selected ToSca10 sites. a) Phase Tensor principle direction rose diagrams for three different period bands b) Phase Tensor skew parameter ($2x\beta$). Values marked in green are below 6, which approximately satisfies 2D necessary conditions. High skew values indicated with red colour indicate 3D effects.

6. 2D inversion

Initially, we started our interpretation of 2017 field data using 2D inversion. Later on, when additional data were available from 2018 field campaign, we inverted all the data using a 3D approach. For the 2D analysis, we have selected 32 sites measured during 2017 field campaign in the period range from 0.003 to 1000 s. The impedance tensor was transformed to the effective apparent resistivity (the determinant of the impedance tensor) and the impedance phase. The profiles directions were selected to coincide with the site locations, due to ambiguity in identifying the strike direction from the impedance tensor alone as well as an inconsistent strike for different period ranges. Generally, 2D inversion must be run along the profiles perpendicular to the geoelectric strike direction, independent of the site locations. Previous results (Pedersen & Engels 2005; Smirnov & Pedersen 2009) of a 2D inversion of the determinant of the impedance tensor showed that the use of the determinant mitigates some of the distortions due to inadequate selection of the strike direction, tensor decomposition into TE and TM modes and inherent 3D effects. However, the underlying assumption of the structure to be 2D seems to be violated anyhow based on the high skew values (Fig. 5a). Therefore, the results of the 2D inversion should be interpreted with care and mostly provide support for our 3D inversion results. With respect to geological (and geoelectric strike deduced after results of 3D inversion) strike directions it seems that profiles 1 and 2 are closest to the orthogonal direction against the strike.

MT sites of the *Profile1* (main profile crossing the Atnsjø tectonic window) were projected onto N50W directed profile, which is very close to being orthogonal to the identified principal direction of N30E of the impedance tensor in the period range $T < 10$ s. We have chosen the direction so that it goes through the actual site locations. The inversion started from a homogeneous half-space with a resistivity of 1000 Ωm and grid size of 180x77 cells (total size of the model 1000x1000km including padding cells to accommodate homogeneous 1D boundary conditions). The error floors were set to 10% for the apparent resistivities and 3° for the phases of the determinant of the impedance tensor data. We have followed a similar approach to invert data along *Profile2* (oriented N10W) and *Profile3* (oriented N-S). The model grid size of these two profiles is 113x68 and 154x81 cells respectively.

We have used REBOCC inversion code by Siripunvaraporn & Egbert (2000) with modifications by Pedersen & Engels (2005) to allow for the inversion of the determinant of the impedance tensor. The final OCCAM type data space inversion results are presented in Fig. 6. Data along all three profiles were fit to normalize (using error floors and actual random data errors) RMS data misfit of 1, which was set as a goal for the constraint inversion process.

All models exhibit common features, namely resistive upper crust up to at least 10 000 Ωm and getting to a more conductive regime at around 10-20 km depth. The similarity of the models gives some confidence in our results. However, it should be noted that many sites are coincident between the profiles. Also, it appears that no strong effect of erroneous profile directions (strike assumption) is evident. Another common feature is the presence of more conductive middle crust, which could be an artefact caused by the effect

of outside of the measurements area structures (conductors). It is indicated by high skew values in the period range of 0.1 – 10 s. The presence of the conductive upper crustal anomaly was previously observed by Cherevatova (2014), and this confirms their findings. Overall, the models are very similar and conform to similar behaviour.

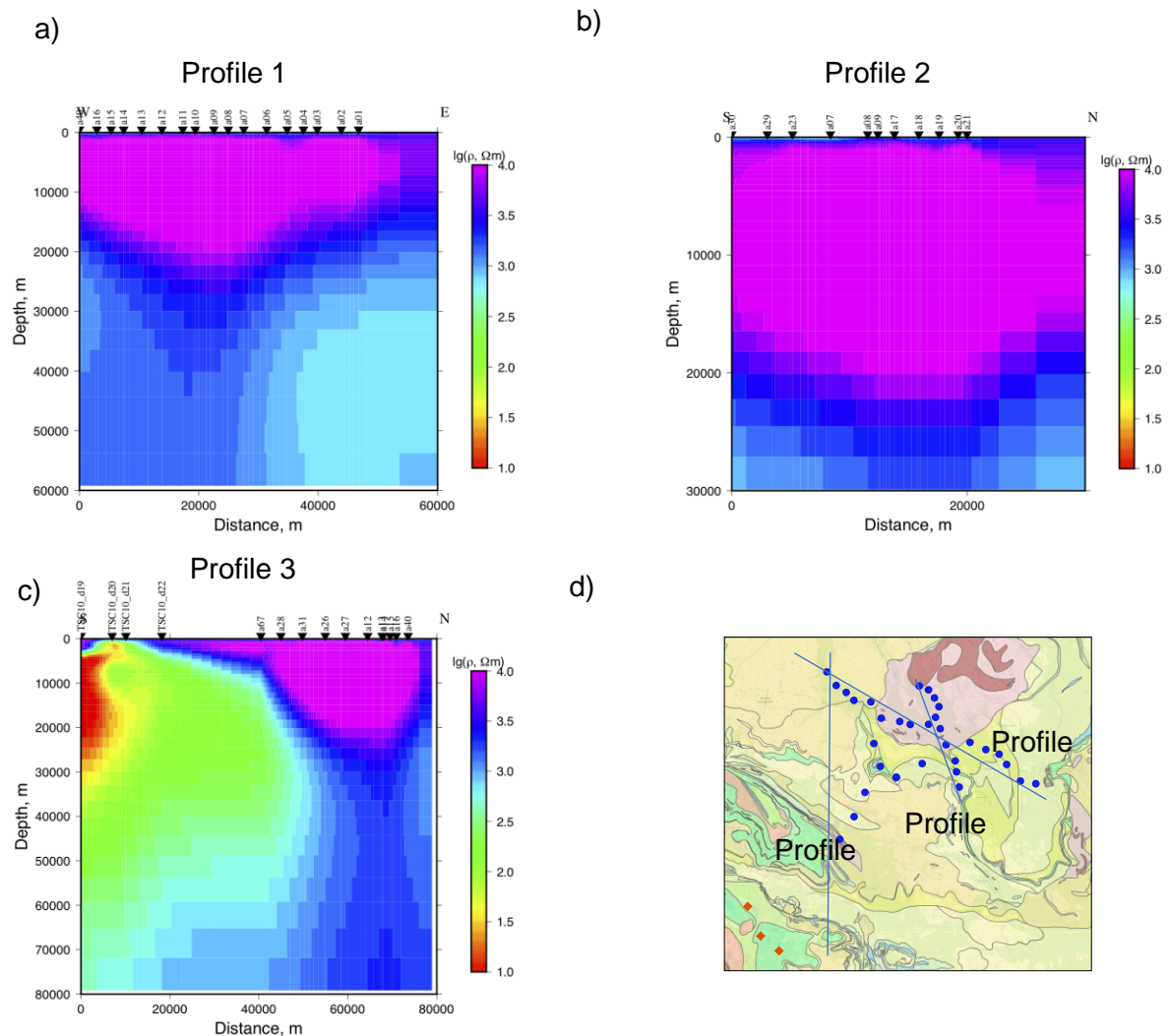


Figure 7: The results of the inversion of the determinant of the impedance tensor along three profiles. a) Profile1 b) Profile2 c) Profile3 d) The positions of the sites and profiles on the geological map (see more details in Fig. 1). Sites from 2017 field campaign are marked with blue dots and red squares indicate ToSca10 sites.

3D inversion

The dimensionality analysis revealed a rather strong 3D effect; therefore 3D inversion is a preferable choice, especially after we have completed the second field campaign. Unlike in 1D or 2D situation, where dispersion relations (Weidelt & Kaikkonen, 1994) can be used as a tool to check the data quality, no such simple relations exist to recognize data affected by noise from realistic 3D response. We have checked data consistency between

adjacent sites and made sure to exclude any part of the data with abrupt variations with frequency. For example, the determinant phase from adjacent sites should converge and the determinant apparent resistivity curves should have an identical shape at sufficiently long periods (long periods sense the same structure due to large penetration depth). 3D inversion in general computationally demanding and running many trails is not yet practical. Therefore, we used only data having passed quality control, which was more stringent than for 2D inversion. After applying this rigorous quality check, we used 75 sites out of 78 with a few sites having limited period range (noisy frequencies were excluded from further analysis).

Several inversion runs have been tested with different input parameters (e.g. starting model, regularization parameters (smoothing factors), model discretization, period range for data, error floor. This, in turn, can also be considered as a sensitivity test for our final model. We used a prior starting model of 1000 Ωm halfspace in all our trails. The final result was obtained on the grid size of 100x100x51. An important parameter of the regularized occam type inversion is the model covariance matrix or roughening operator (the inverse of the square root of the covariance matrix). The covariance operator defines the type of regularization term and smoothness of the model, which can be considered as sort of a priori information imposed on the model domain search. We have used MODEM software for 3D inversion (Egbert & Kelbert, 2012), which allows for the auto-regression type covariance matrix, thus providing smooth models. The smoothness is defined independently in X, Y and Z directions with scaling factor varying 0.1-0.5 (other values are possible but the converge would be affected). The smoothness of 0.3 in all directions is a default value in MODEM. We have tried various smoothness values, including increasing horizontal smoothing to emphasize layered structures and less smoothness in the vertical direction. However, the best data fits were consistently achieved using a higher smoothing factor of 0.5 instead of the default 0.3 in horizontal directions. During iterations, the smoothing operator was applied three times. For the preferred model, the input data consisted of full impedance tensor \mathbf{Z} (all 4 components) (0.003–100 s, 4 periods/decade). The error floor was set to 5% of the main off-diagonal impedance components. Additional impedances (diagonal components xx,yy) were assigned corresponding absolute values of error floors from their raw matching main impedances (xy,yx). The argument behind setting up the error floor for the additional impedances comes from a general consideration of the regression problems, for example, for the first row of the impedance tensor:

$$\mathbf{E}_x = Z_{xx}\mathbf{H}_x + Z_{xy}\mathbf{H}_y + \epsilon,$$

where ϵ is a noise component in a predicted variable \mathbf{E}_x . Predictors (input) variables \mathbf{H} are considered to be noise free. The data covariance matrix is defined as

$$\text{Cov}(\mathbf{Z}) = \sigma^2(\mathbf{H}^*\mathbf{H})^{-1}, \text{ where } \sigma^2 \text{ is a noise variance.}$$

Assuming that there is no preference in the polarization of the incident field we may conclude that the variance for both Z_{xx} and Z_{xy} will be the same (as an absolute value). Therefore, when using the error floor, we must apply the same absolute error to both components and derive this absolute value from dominant main components.

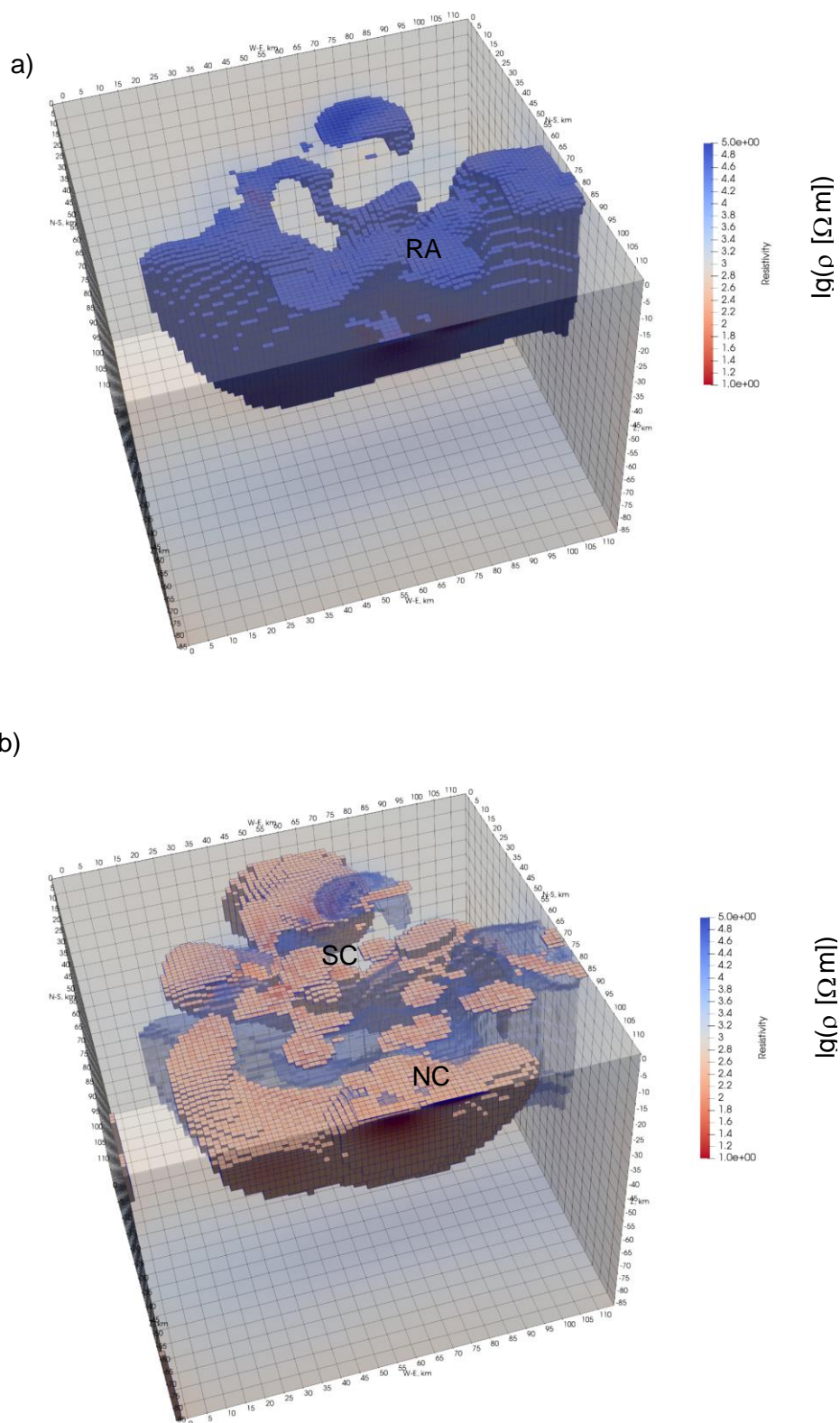


Figure 8: The result of 3D inversion of the full impedance tensor using the ModEM inversion algorithm. (a) Middle resistive anomaly is shown as iso-surfaces of 10000 Ωm (RA). (b) Additionally, to (a) conductors are depicted with iso-surfaces of 100 Ωm to the south (SC) and to the north-west (NC).

Within the rectangular area covered by the sites, the grid was discretized into 1300x1300

m cells in the horizontal direction. Outside the array the cell sizes were increased by a factor of 1.2 towards the outer edges in order to fulfill Dirichlet boundary conditions in the forward computation. In vertical direction cells in the topmost layer have a thickness of 50 m and the thickness of subsequent cells increase with a factor of 1.1 towards greater depths with the model bottom at ca. 1000 km. The smoothing factors were set to 0.5 in both X and Y directions and in Z direction were set to 0.3. The less smoothing used in the vertical direction allows to better delineate the depth extend of the anomalies at the same time emphasizing the laterally extending structures.

The results of 3D inversion are supported by the results of 2D inversions (which might be biased due to 3D effects). In the middle of the array, highly resistive area (RA) stretching from west to east is detected from the surface down to at least middle crust (Figs. 7, 8, 9 & 10), coinciding with the location of Gudbrandsdalen Anticline. There are two major conductive regions in the model. The northern conductor (NC) matches Upper allochthon greenstones where black schists and sulphide mineralisations occur. The southern conductive area (SC) depicts the Fåvang basin.

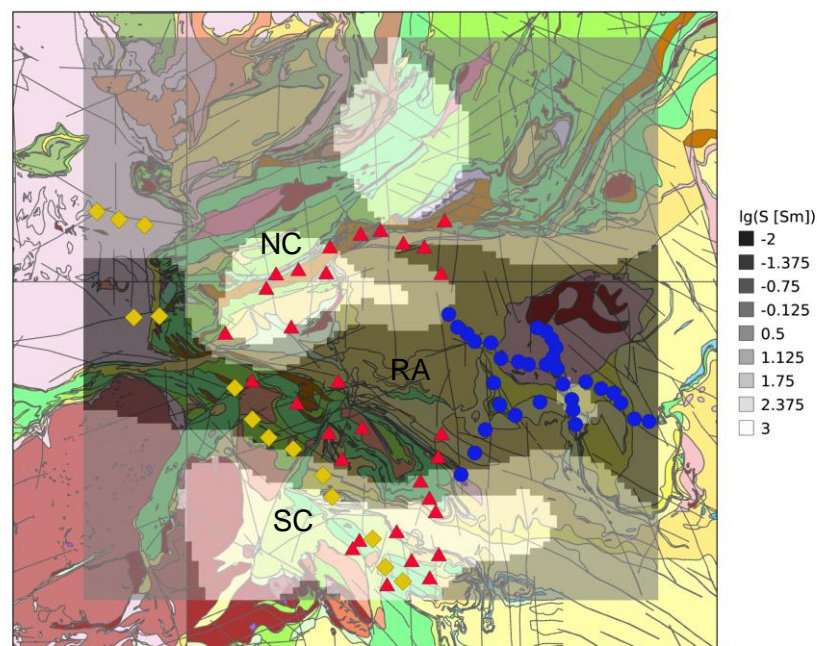


Figure 9: A 3D model slice of the integrated conductance at the depth range of 5-10 km. The resistor in the middle of the area (RA) coincides with the Middle Allochthon. Conductors are located to the south (SC) and to the north (NC). The conductors to the south are also clearly indicated in the longer Profile2 inversion, which includes a few sites from the ToSca10 data set. See legend in Fig. 1.

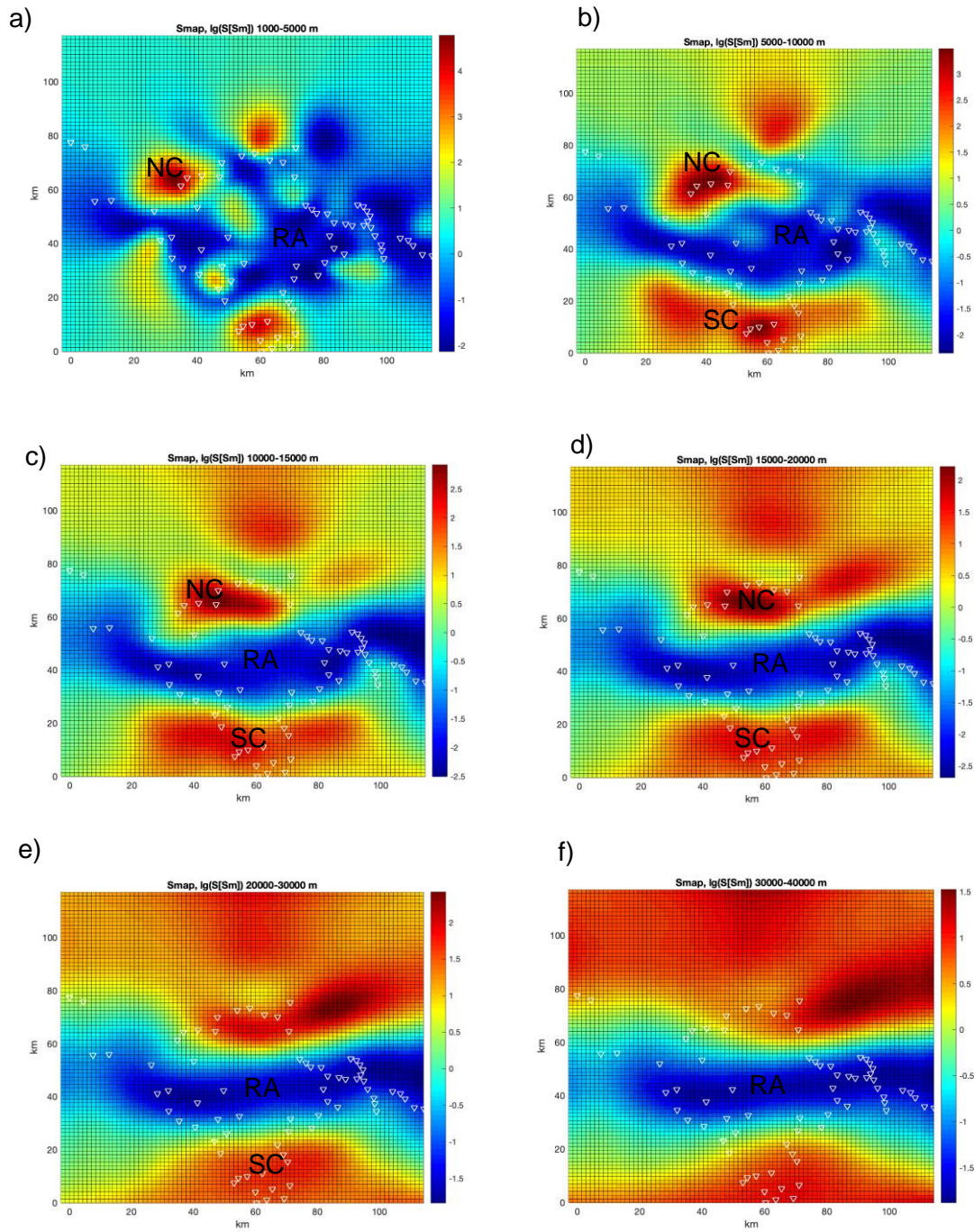


Figure 10: 3D model slices of the conductance at different depth ranges. The study area is resistive in the middle (RA). The model has no strong conductive anomalies. However, 3D inversion indicates the presence of conductors to the south (SC) and to the north (NC). The conductors are located to the south and to the north-west of the area, which is also known from a previous study (Cherevatova, 2014) in the area. The conductors to the south are also clearly indicated in the longer Profile2 inversion, which included a few sites from the ToSca10 data.

3D inversion results are very much dependent on the distribution and density of the available data. Some of the artefacts due to sparse availability (inhomogeneous distribution of the data) are mitigated by the smoothness constraints. Therefore, some localized conductors, if not well covered from all the sides, might have erroneous shape, especially those located close to the modelling domain boundaries. Those conductors may extend further away in reality. Therefore some of the shapes of the observed conductors may not be exact, due to limited data coverage.

One of the best resolved parameters in magnetotellurics is conductance. Therefore, it is useful to present maps of conductance slices for various depths. On Fig. 10 six slices are shown, which in another way confirm the observations made previously. The structures observed in the model in the first km could be affected by the galvanic effects (to resolve the issue, denser coverage is required), whereas at greater depth the model is much more consistent and therefore more robust.

7. Discussion and conclusions

New high-quality magnetotelluric (MT) data were acquired in the Rondane region during two field seasons. An array of 33 broad-band magnetotelluric sites were measured in September 2017, and 32 sites were added in the following summer 2018, i.e. in total 65 sites. During the measurement period of 2017, geomagnetic activity was at a high level, which resulted in high signal to noise ratio. This fact explains the relatively high data quality. Subsequently, the resulting MT transfer functions estimated using the multi remote reference technique in the period range from 0.003 to 1000 s have good to excellent quality. During the summer 2018 field campaign, more sites were affected by local cultural noise, however, still, most of the sites had rather high quality (see Appendix A and B, showing apparent resistivity and phase for all the sites.). The Phase Tensor analysis was used to estimate the strike and dimensionality of the MT data. Dimensionality and strike analyses indicate noticeable 3D effects especially in the period band 0.1-10 s. The principal direction of the impedance tensor can be identified; however, it varies with period. For the 2017 data inversion, we firstly chose to invert in 2D the determinant of the impedance tensor, which mitigates 3D effects under 2D model assumptions. Furthermore, we performed a full 3D inversion of all the available data in the area.

Three crustal-scale 2D models are selected and analysed only for the first-year field campaign when limited data were available. We have chosen to invert data in three different strike directions due to 90° ambiguity in strike determination and uncertainty in the determination of the principle direction. The results of 2D inversion, however, are consistent between all the profiles. Furthermore, due to significant 3D effects in the data, we have selected to invert the larger array, including the data from two field seasons and previously acquired ToSca10 sites available in the area, using full impedance tensor 3D inversion. It resulted in an acceptable data fit and robust model. Hence, we base our interpretation on the 3D inversion results. All the models we have tested show a highly resistive deep-seated approximately E-W elongated unit in the middle of our array (RA in

Figs. 8a, 9 & 10). This anomaly correlates with the E-W trending Gudbrandsdalen Anticline (Sturt & Ramsay, 1997) and with a shallow depth to the Precambrian basement inferred from gravity data (Fig. 2). The resistivity of the upper crust is around 10 000 Ω m and starts to decrease at a depth of 20 km (Fig. 8).

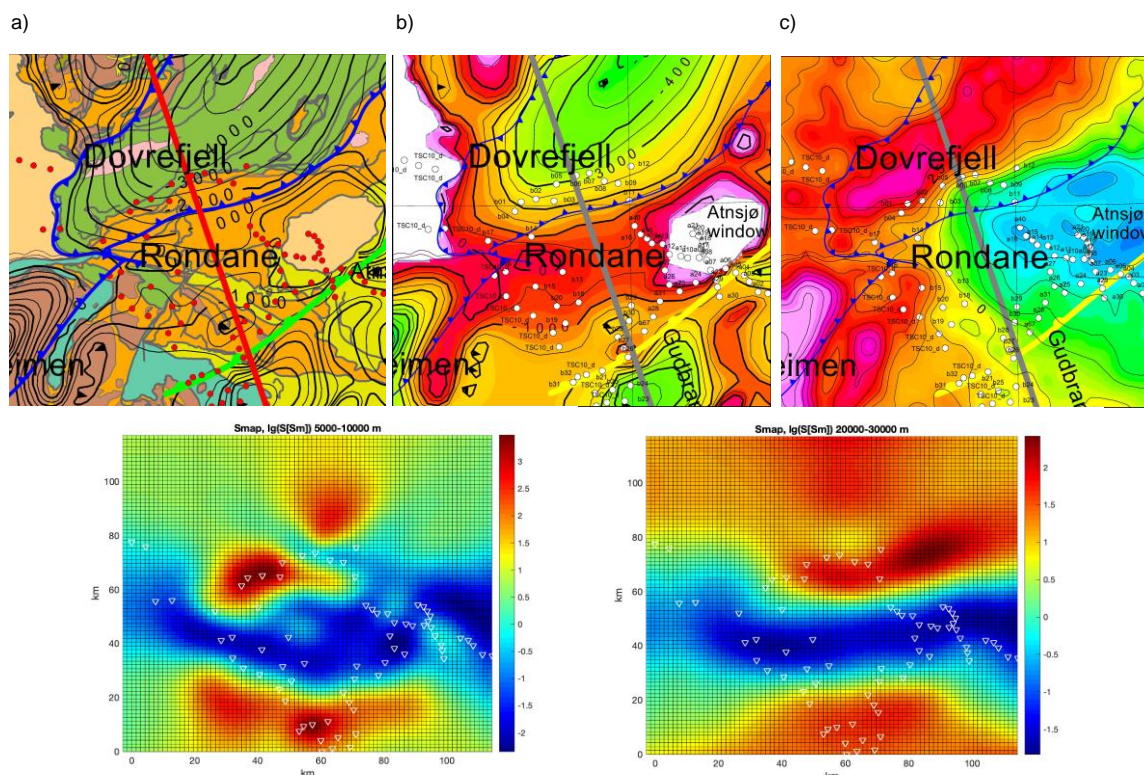


Figure 11. Comparison of integrated conductance maps over the depth of 5-10 and 20-30 km with the tectonic map (a), depth to the basement map (b) and gravimetric isostatic residual map (c) (see legends in Figs. 2 and 10b,e).

The Gudbrandsdalen Anticline (Figs. 2 & 11) was formed during Devonian thrusting of the basement windows (Lower Allochthon). The older, Silurian thrusting of the Middle Allochthon is refolded.

Resistive rocks, extending to the surface in the Gudbrandsdalen Anticline image the parautochthonous Western Gneiss Region to the west and Middle Allochthon in the middle and to the east of the area (Fig. 2). In ToSca'10, the Caledonian nappes, the conducting black schists and the deeper conductor are terminated in the west and north by the Devonian detachments extending from Hardangerfjorden through Jotunheimen to Røros in the northeast (incl. the Faltungsgaben shear complex and the Lærdal-Gjende Fault). The structures represent a crustal scale boundary between the Western Gneiss Region in the northwest and the Southwest Scandinavian Domain in the southeast. This is also supported by the 3D inversion model, which provides more details about the complex three-dimensional structure of the area. Thus, in the Rondane-Gudbrandsdalen region, the WGR and Middle Allochthon appears as a highly resistive unit until the southeastern border of the Caledonian nappes that are cut by the Devonian detachments to the northwest. The main detachment structures coincide with a conductive anomaly which extends through nearly the whole crust. The Atnsjø tectonic window appears to be the part of resistive Middle Allochthon that included in the Gudbrandsdal Anticline and cannot be separated from it, based on conductivity model alone. We conclude that highly conductive black schists and alum shales are absent in the Atnsjø tectonic window.

8. References

- Andersen, T. B. 1998: Extensional tectonics in the Caledonides of southern Norway, an Overview. *Tectonophysics* 285, 333 – 351.
- Andersson, A., Dahlman, B., Gee, D.G. & Snall, S. 1985: The Scandinavian alum shales. *Sveriges Geologiska Undersökning (SGU), Serie Ca, NR, 56*, 1–49.
- Bahr, K. 1991: Geological noise in magnetotelluric data: a classification of distortion types. *Physics of the Earth and Planetary Interiors* 66(1-2), 24 – 38.
- Berdichevsky, M. & Dmitriev, V. 1976: Basic principles of interpretation of magnetotelluric sounding curves. In A. Adam (ed.): *Geoelectric and Geothermal Studies*. Akademiai Kiado, Budapest, Hungary. *KAPG Geophysical Monograph*, pp. 165_221.
- Berdichevsky, M., Pokhotelov, D., 1997. Violation of the dispersion relations in a three-dimensional magnetotelluric model. *Izvestiya, Phys. Solid Earth* 33, 603–608.
- Bergström, J. & Gee, D. G. 1985: The Cambrian in Scandinavia. In Gee, D. G. & Sturt, B. A. (eds.): *The Caledonide Orogen - Scandinavia and Related Areas*, 247-271. John Wiley & Sons Ltd, Chichester.
- Bingen, B., Stein, H. J., Bogaerts, M., Bolle, O. & Mansfeld, J. 2006: Molybdenite Re-Os dating constrains gravitational collapse of the Sveconorwegian orogen. SW Scandinavia. *Lithos* 87, 328–346.
- Bingen, B., Nordgulen, Ø. & Viola, G. 2008a: A four-phase model for the Sveconorwegian orogeny, SW Scandinavia. *Norwegian Journal of Geology*, 88, 43–72.
- Bingen, B., Andersson, J., Soderlund, U. & Möller, C. 2008b: The Mesoproterozoic in the Nordic countries, *Episodes* 31(1), 29–34.
- Bjørlykke, A. & Olesen, O. 2018: Caledonian deformation of the Precambrian basement in southeastern Norway. *Norwegian Journal of Geology* 98, 1-16. <https://dx.doi.org/10.17850/njg98-4-05>.
- Boerner, D.E., Kurtz, R.D. & Craven, J.A. 1996: Electrical conductivity and Paleoproterozoic foredeeps. *J. Geophys. Res.* 101(B6), 13775–13791.
- Brasse, H., Kreutzmann, A., Cerv, V., Ernst, T., Jankowski, J., Jozwiak, W., Neska, A., Pedersen, L. B. Smirnov, M., Schwarz, G., Sokolova, E., Varentsov, I. M., Hoffmann, N., Palshin, N. & Korja, T. 2006: Probing electrical conductivity of the Trans-European suture zone. *Eos Trans. AGU* 87(29), p 281.
- Cherevatova, M., Smirnov, M., Korja, T., Kaikkonen, P., Pedersen, L.B., Hübert, J., Kamm, J. & Kalscheuer, T. 2014: Crustal structure beneath southern Norway imaged by magnetotellurics. *Tectonophysics* 628, 55-70.
- Cherevatova M., Smirnov, M., Korja, T., Ebbing J., Gradmann S., Becken, M. & MaSca Working Group 2015: Electrical conductivity structure of the north-west Fennoscandia from three-dimensional inversion of magnetotelluric data. *Tectonophysics* 653, 20-32.
- Ebbing, J., England, R., Korja, T., Lauritsen, T., Olesen, O., Stratford, W. & Weidle, C. 2012: Structure of the Scandes lithosphere from surface to depth. *Tectonophysics* 536 -537, 1 – 24.
- Egbert, G.D. & Kelbert, A. 2012: Computational recipes for electromagnetic inverse problems. *Geophysical Journal International*, 189(1), 251–267.
- England, R.W. & Ebbing, J. 2012: Crustal structure of central Norway and Sweden from integrated modelling of teleseismic receiver functions and the gravity anomaly. *Geophysical Journal International*, doi: 10.1111/j.1365-246X.2012.05607.x
- Frost, B. R., Fyfe, W. S., Tazaki, K. & Chan, T. 1989: Grain-boundary graphite in rocks and implications for high electrical conductivity in the lower crust, *Nature*, 340, 134-136.
- Gaál, G. & Gorbatshev, R. 1987: An outline of the Precambrian evolution of the Baltic Shield. *Precambrian Research* 35, 15 – 52.
- Gee, D. 2005: Scandinavian Caledonides (with Greenland). *Elsevier Encyclopedia of Geology* 2, 64–74.
- Gee, D. & Sturt, B. 1985: The Caledonide orogen – Scandinavia and Related Areas. *John Wiley & Sons, Chichester*. 1266 pp.
- Gee, D. G. 1972: The regional geological context of the Tasjo Uranium Project, Caledonian Front, Central Sweden. *Sveriges Geologiska Undersökning (SGU), Serie C(671)*, 1–36.
- Gee, D. G. 1980: Basement-cover relationships in the central Scandinavian Caledonides. *Geologiska Föreningen i Stockholm Handlingar* 102(4), 455–474.
- Gorbatshev, R. & Bogdanova, S. 1993: Frontiers in the Baltic Shield. *Precambrian Research* 64, 3–21.

- Grad, M., Tiira, T. & Group, E.W. 2009: The Moho depth map of the European Plate. *Geophysical Journal International* 176, 279–292.
- Heeremans, M., Larsen, B. T., & Stel, H., 1996. Paleostress reconstruction from kinematic indicators in the Oslo Graben, southern Norway: new constraints on the mode of rifting. *Tectonophysics*, 266(1), 55–79.
- Koistinen, T., Stephens, M.B., Bogatchev, V., Nordgulen, Ø., Wennerstrøm, M. & Korhonen, J., 2001. Geological map of the Fennoscandian Shield, scale 1:2,000,000. *Geological Surveys of Finland, Norway and Sweden and the Northwest Department of Natural Resources of Russia*.
- Korja, T. 2007: How is the European Lithosphere Imaged by Magnetotellurics? *Surveys in Geophysics* 28, 239 – 272.
- Korja, T. & Koivukoski, K. 1994: Crustal conductors along the SVEKA Profile in the Fennoscandian (Baltic) Shield, Finland. *Geophysical Journal International*, 116(1), 173–197.
- Korja, T., Engels, M., Zhamaletdinov, A., Kovtun, A., Palshin, N., Tokarev, A., Smirnov, M., Asming, V., Vanyan, L., Vardaniants, I., & Bear, W.G. 2002: Crustal conductivity in Fennoscandia - a compilation of a database on crustal conductance in the Fennoscandian Shield. *Earth Planets Space* 54, 535–558.
- Korja, T., Smirnov, M., Pedersen, L. & Gharibi, M. 2008: Structure of the Central Scandinavian Caledonides and the underlying Precambrian basement, new constraints from magnetotellurics. *Geophysical Journal International* 175, 55 – 69.
- Mekonnen, A.Y. 2004: *A geophysical study of the Central Norwegian Caledonides*. MSc. thesis, NTNU, Trondheim, 80 pp.
- Norton, M.G, McClay, K.R. Way, N.A. 1987: Tectonic evolution of Devonian basins in northern Scotland and southern Norway. *Norsk Geologisk Tidsskrift* 67, 323-338.
- Olesen, O., Brønner, M., Ebbing, J., Gellein, L., Gernigon, L., Koziel, J., Lauritsen, S., Myklebust, R., Pascal, C., Sand, M, Solheim, D. & Usov, S. 2010: New aeromagnetic and gravity compilations from Norway and adjacent areas: methods and applications. In Vining, V.A. & Pickering, S.C. (eds.): *Petroleum geology: From mature basins to new frontiers - Proceedings from the 7th Petroleum Geology Conference*, Geological Society of London, pp. 559–586.
- Pedersen, L.B. & Engels, M. 2005: Routine 2D inversion of magnetotelluric data using the determinant of the impedance tensor. *Geophysics* 70, G33–G41.
- Pérez, E.C. 2015: The Lærdal-Gjende Fault: A detailed structural and thermochronological study. Master thesis, University of Bergen, 193 pp.
- Raab, S., Hoth, P., Huenges, E., & Müller, H.J., 1998: Role of sulfur and carbon in the electrical conductivity of the middle crust. *J. Geophys. Res.* 103(B5), 9681–9689.
- Ramberg, I.B., Bryhni, I., Nøttvedt, A. & Rangnes, K., eds., 2008: The Making of a land – Geology of Norway. Geological Society of Norway, Trondheim, 624 pp.
- Rasmussen, T.M., Roberts, R.G. & Pedersen, L.B. 1987: Magnetotellurics along the Fennoscandian long range profile. *Geophysical Journal of the Royal Astronomical Society* 89, 799 – 820.
- Roberts, D. 2003: The Scandinavian Caledonides: event chronology, palaeogeographic settings and likely modern analogues. *Tectonophysics* 365, 283 – 299.
- Robinson, P., Roberts, D., Gee, D.G. & Solli, A. 2014: A major synmetamorphic Early Devonian thrust and extensional fault system in the Mid Norway Caledonides: relevance to exhumation of HP and UHP extensional fault system in the Mid Norway. In Corfu, F., Gasser, D. & Chew, D.M. (eds): *New Perspectives on the Caledonides of Scandinavia and Related Areas*, Geological Society of London, Special Publications 390, 1–8.
- Røhr, T.S., Bingen, B., Robinson, P. & Reddy, S.M. 2013: Geochronology of Paleoproterozoic Augen Gneisses in the Western Gneiss Region, Norway: Evidence for Sveconorwegian Zircon Neocrystallization and Caledonian Zircon Deformation. *Journal of Geology* 121, 105–128.
- Rykkelid, E. & Andresen, A. 1994: Late Caledonian extension in the Ofoten area, northern Norway. *Tectonophysics* 231, 157–169.
- Siripunvaraporn, W. & Egbert, G. 2000: An efficient data-subspace inversion method for 2D magnetotelluric data. *Geophysics* 65(3), 791 – 803.
- Skilbrei, J.R. 1990: Structure of the Jotun Nappe Complex, Southern Norwegian Caledonides: Ambiguity of gravity modelling and reinterpretation. *NGU Report* 89.169, 26 pp.
- Smirnov, M.Yu. 2003: Magnetotelluric data processing with a robust statistical procedure having a high breakdown point. *Geophysical Journal International* 152(1), 1 – 7.
- Smirnov, M.Yu., Korja, T., Dynesius, L., Pedersen, L.B. & Laukkanen, L. 2008: Broadband magnetotelluric instruments for near-surface and lithospheric studies of electrical conductivity: A Fennoscandian pool of magnetotelluric instruments. *Geophysica* 44(1-2), 15 – 27.

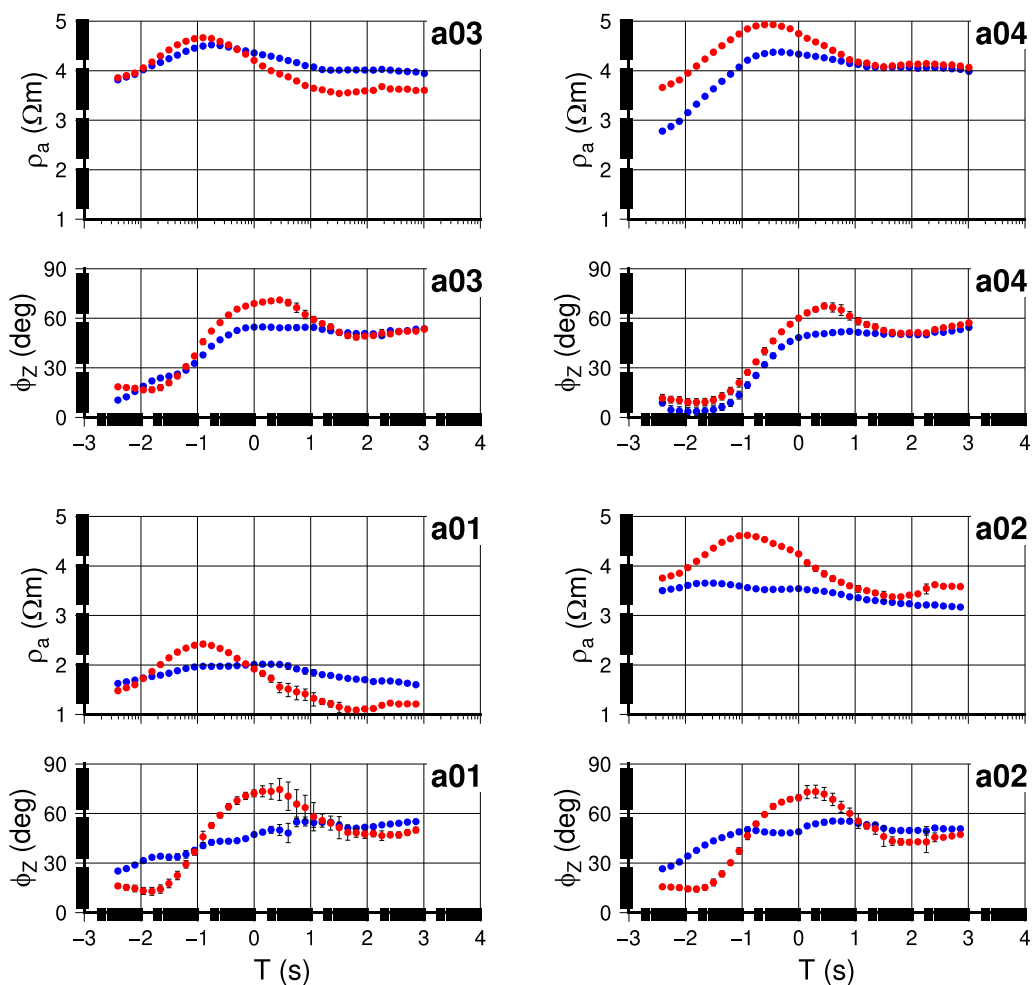
- Smirnov, M.Yu. & Pedersen, L.B. 2009: Magnetotelluric measurements across the Sorgenfrei-Tornquist Zone in southern Sweden and Denmark. *Geophys. J. Int.* 176, 443-456.
- Smirnov, M.Yu. & Egbert, G.D. 2012: Robust principal component analysis of electromagnetic arrays with missing data. *Geophysical Journal International* 190(3), 1423-1438.
- Sturt, B.A. & Ramsay, D. 1997: The Gudbrandsdalen Antiform – a major Late Caledonian structure. *Norges geologiske undersøkelse Bull* 433, 12-13.
- Törnebohm, A.E. 1896: Grunddragen af det Centrala Skandinaviens bergbyggnad. *Kongliga Svenska Vetenskapsakademiens handlingar* 28(1/2 10), in Swedish.
- Weidelt, P. & Kaikkonen, P. 1994: Local 1D interpretation of magnetotelluric B-polarization impedances. *Geophysical Journal International* , 117(3), 733-748.

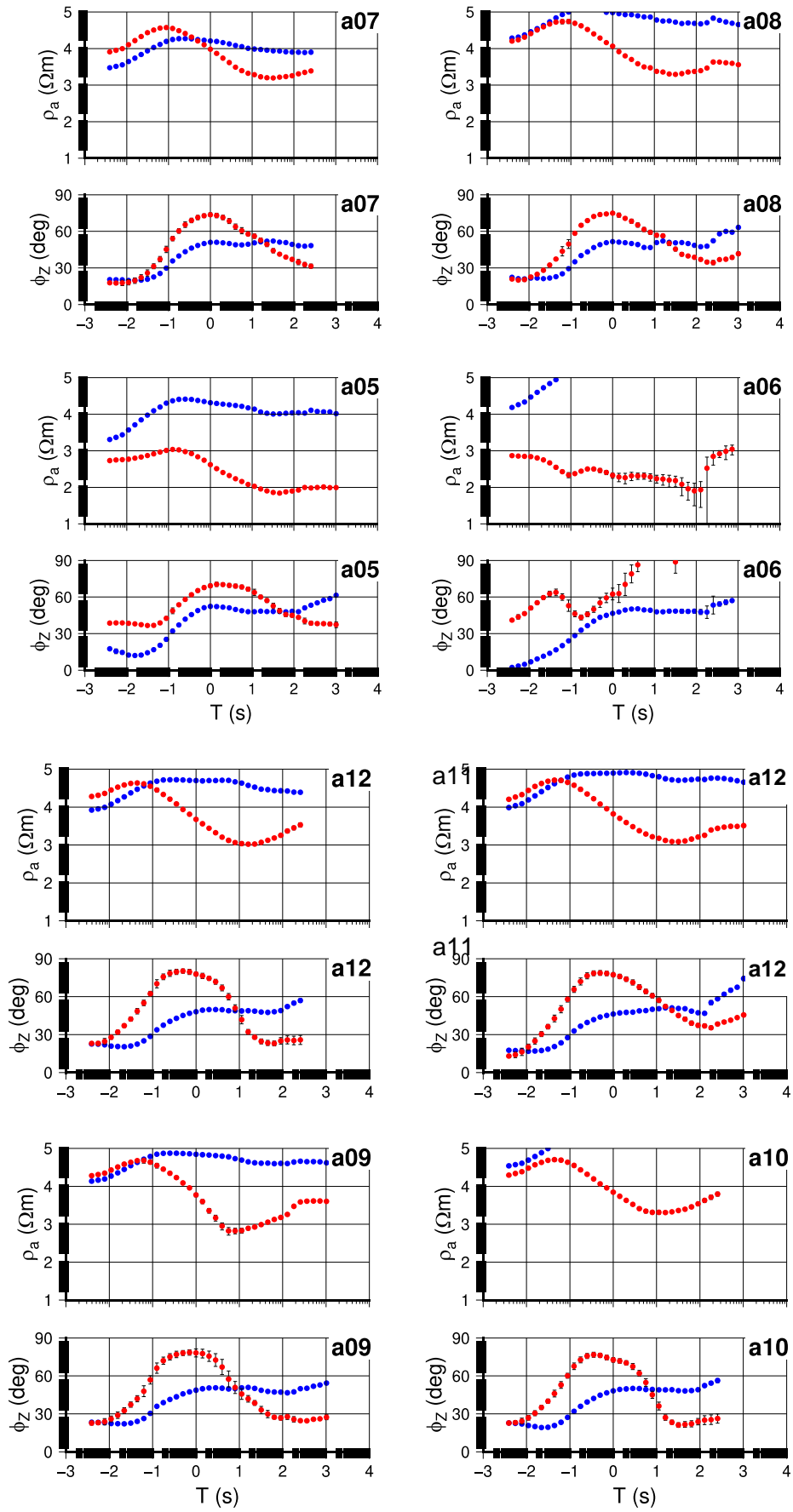
9. Appendices

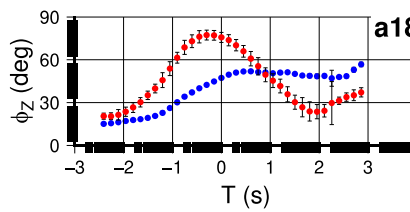
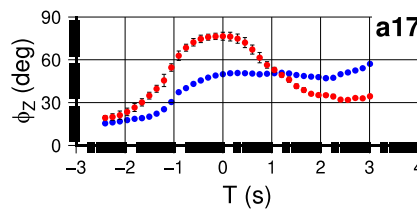
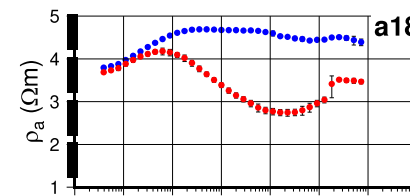
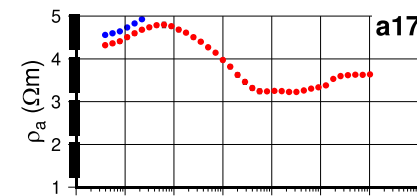
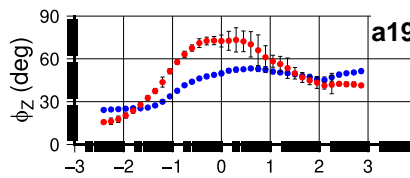
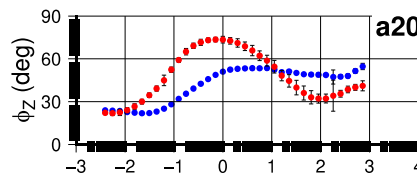
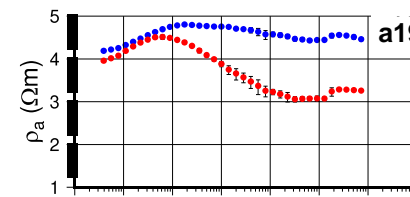
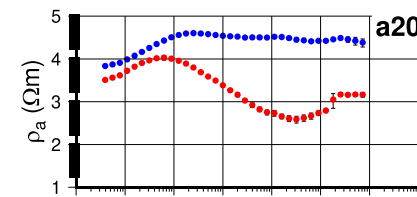
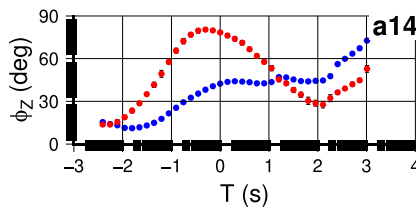
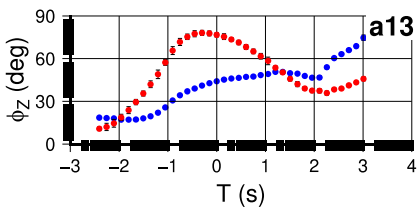
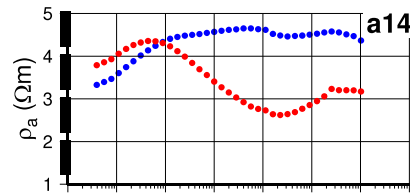
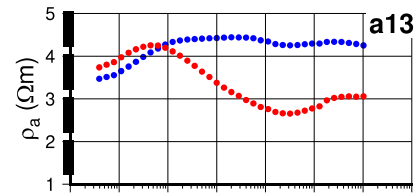
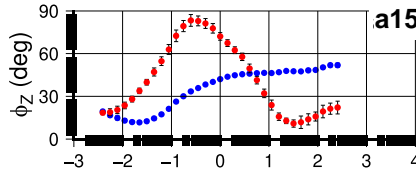
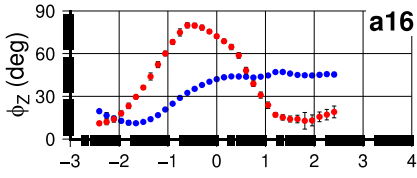
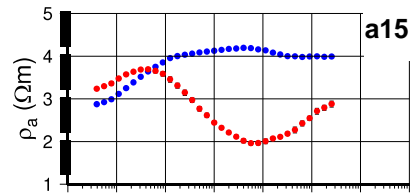
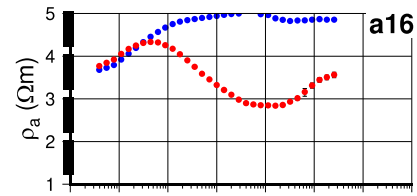
9.1. Appendix A

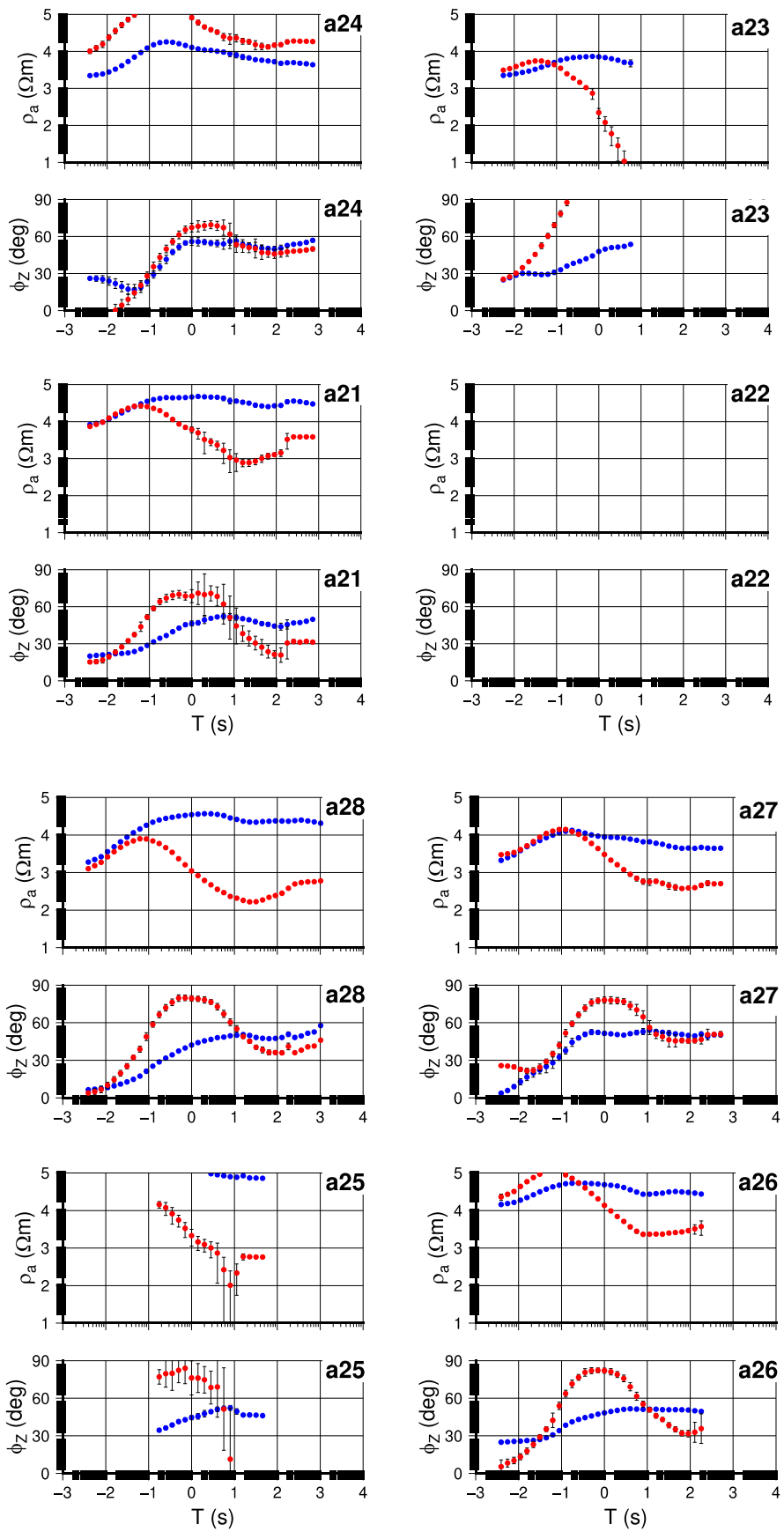
Apparent resistivities and impedance phases at individual sites in the Rondane 2017 field campaign.

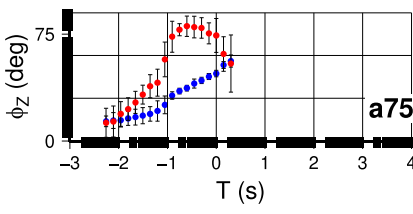
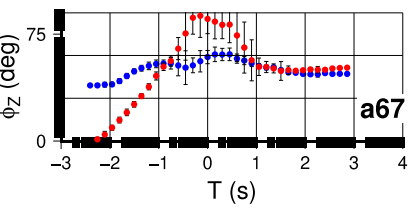
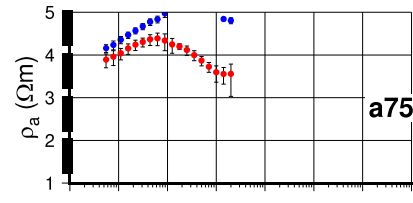
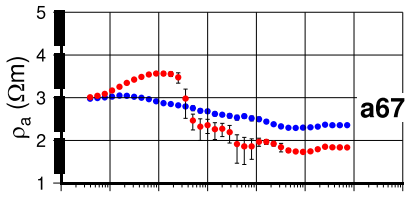
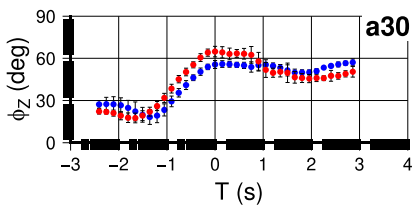
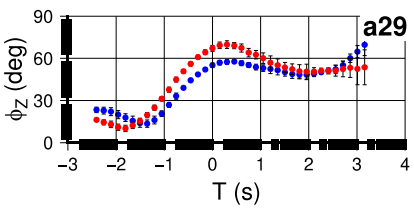
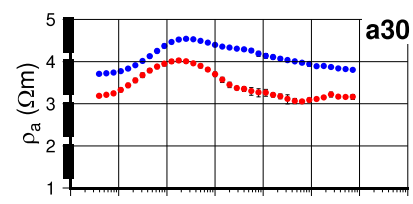
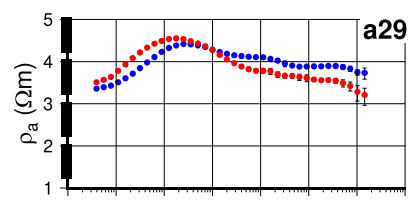
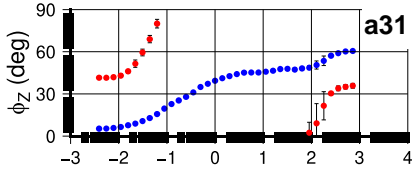
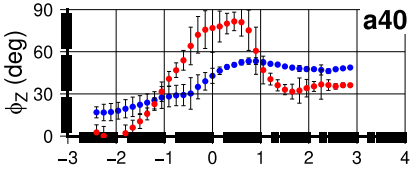
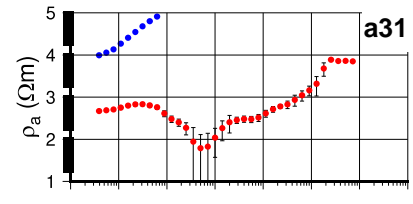
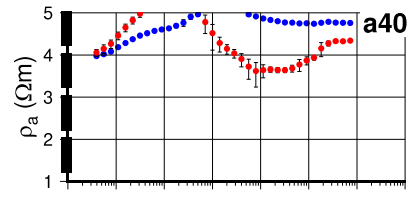
Estimated main components of the impedance tensor, shown as apparent resistivities and impedance phases. Apparent resistivities ρ_{xy} , ρ_{yx} are marked in red and blue circles, respectively, as well as the corresponding impedance phases ϕ_{xy} , ϕ_{yx} .







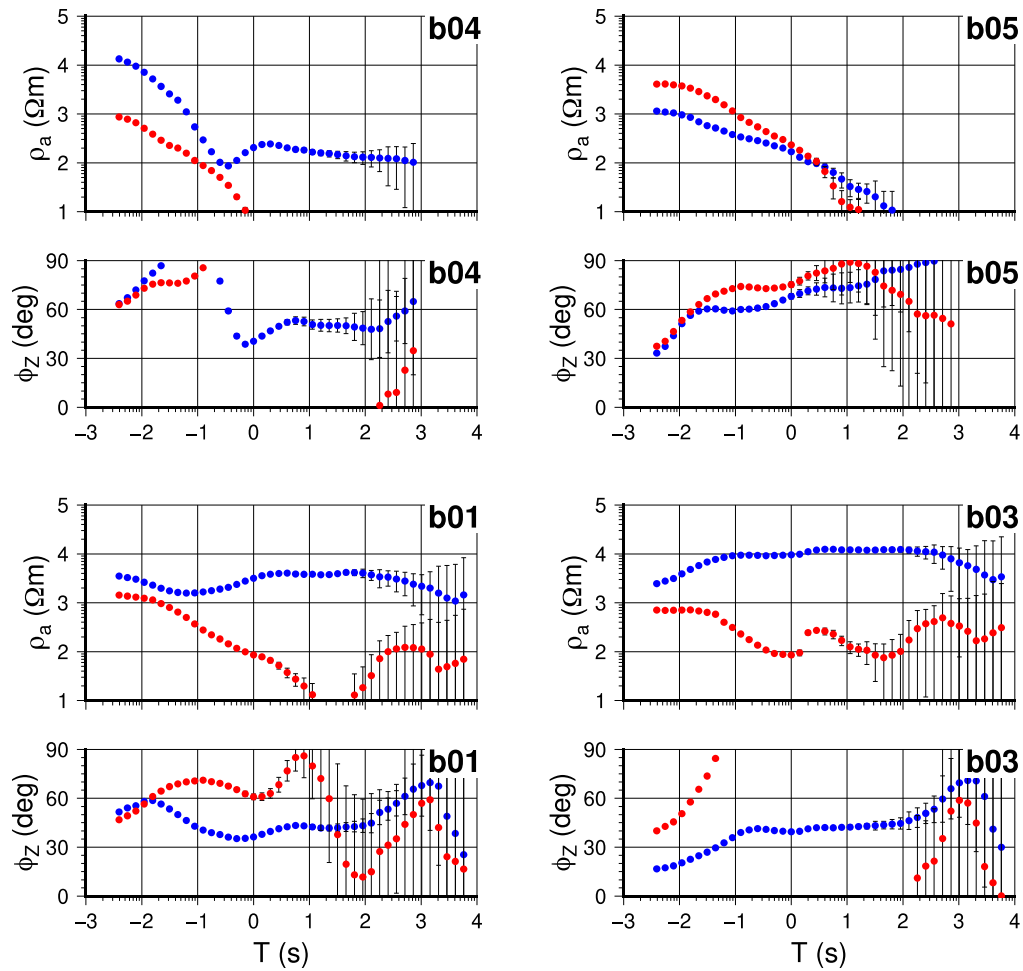


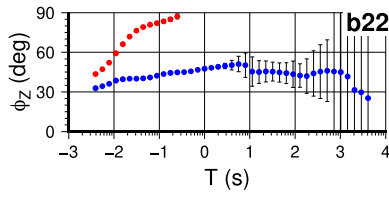
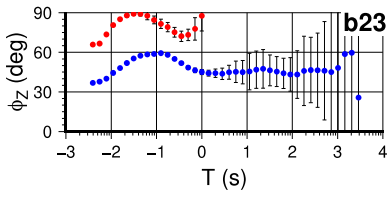
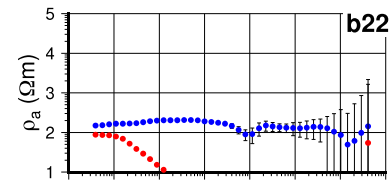
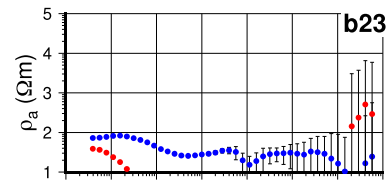
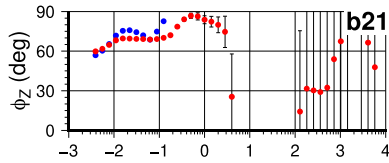
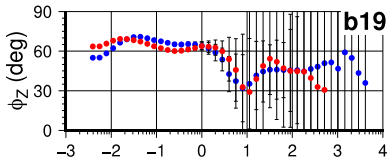
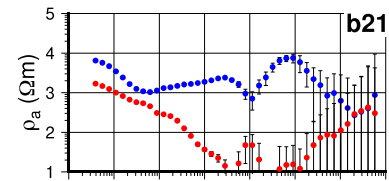
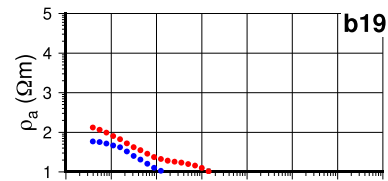
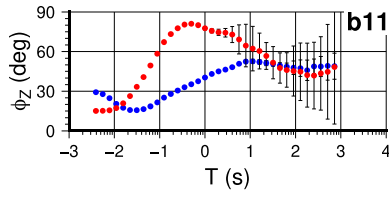
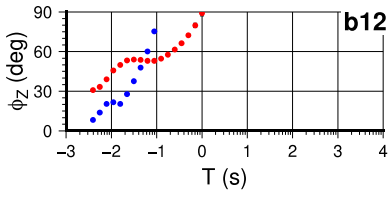
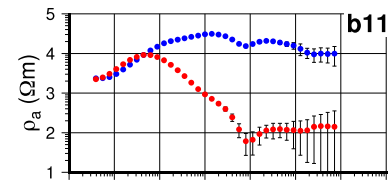
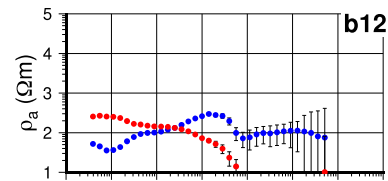
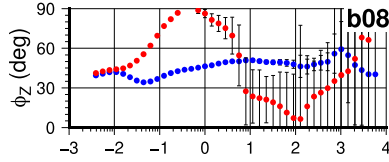
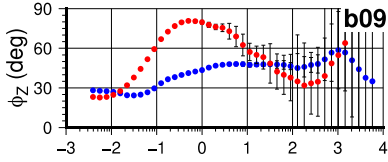
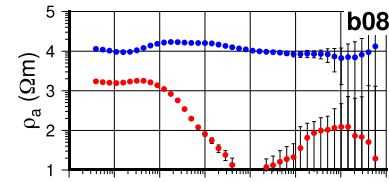
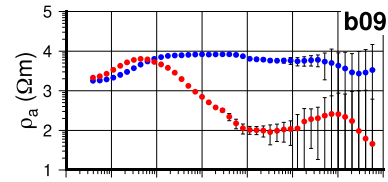


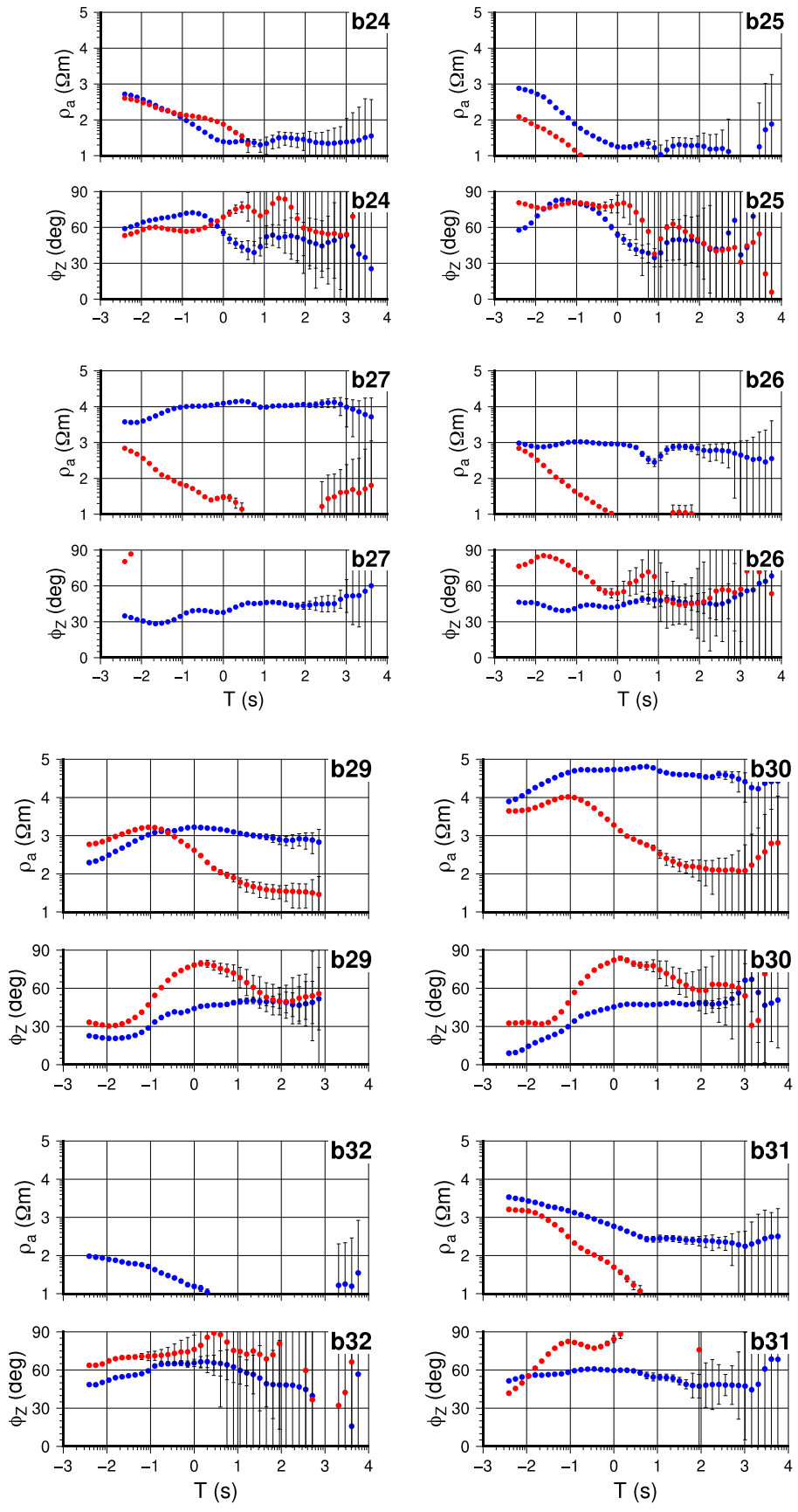
9.2. Appendix B

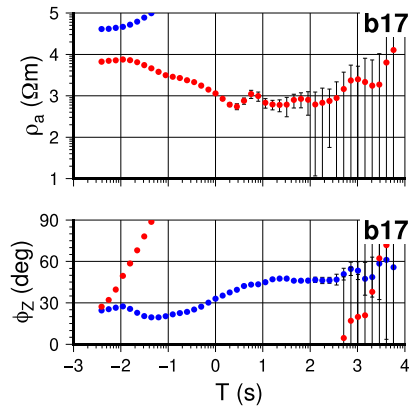
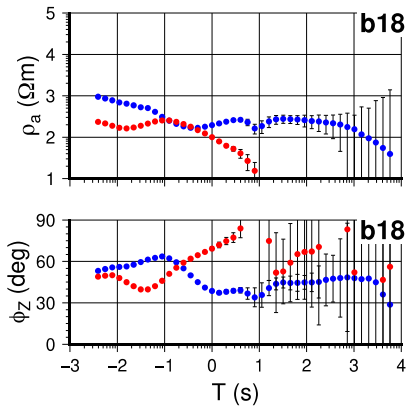
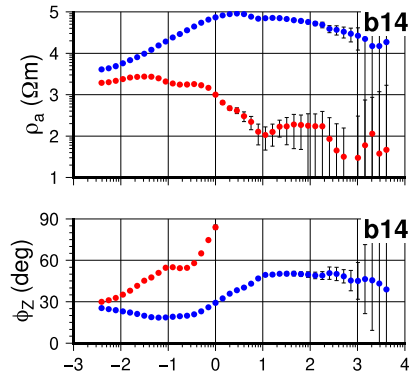
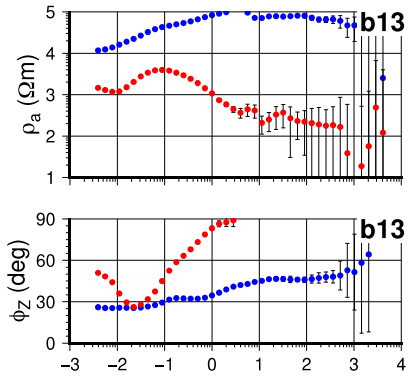
Apparent resistivities and impedance phases at individual sites in the Rondane 2018 field campaign.

Estimated main components of the impedance tensor, shown as apparent resistivities and impedance phases. Apparent resistivities ρ_{xy} , ρ_{yx} are marked in red and blue circles, respectively, as well as the corresponding impedance phases ϕ_{xy} , ϕ_{yx} .











GEOLOGICAL
SURVEY OF
NORWAY

· NGU ·

Geological Survey of Norway
PO Box 6315, Sluppen
N-7491 Trondheim, Norway

Visitor address
Leiv Eirikssons vei 39
7040 Trondheim

Tel (+ 47) 73 90 40 00
E-mail ngu@ngu.no
Web www.ngu.no/en-gb/